A MODEL STUDY OF WIND FORCES ON HYPERBOLIC PARABOLOID SHELLS

By

KARLSON EDDY MANNSCHRECK

Bachelor of Science

Oklahoma State University

Stillwater, Oklahoma

1963

Submitted to the faculty of the Graduate School of
the Oklahoma State University
in partial fulfillment of the requirements
for the degree of
MASTER OF SCIENCE
May, 1964

A MODEL STUDY OF WIND FORCES

ON HYPERBOLIC PARABOLOID

SHELLS

Thesis Approved:

Thesis Advisor

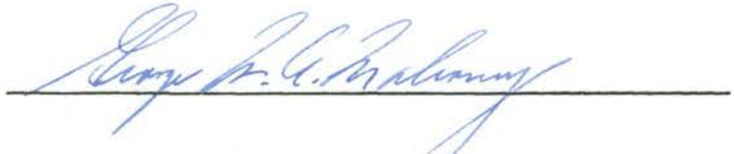

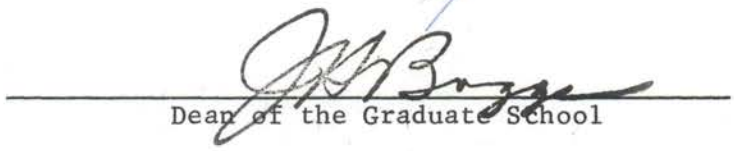

Dean of the Graduate School

PREFACE

The use of various configurations of concrete shells has rapidly been accepted by the American public in recent years. The hyperbolic paraboloid type of structure is becoming more common due to its versatility, ease of construction, and relatively low cost. To have an efficient as well as functional design, a knowledge of the wind forces which will be developed on the structure is necessary.

The purpose of this study is then to determine the wind forces acting on one configuration of hyperbolic paraboloid shell and to determine the factors affecting these forces.

Indebtedness is acknowledged to Doctor G. L. Nelson for his guidance and encouragement throughout the study; also to Oklahoma State University and the Oklahoma Agricultural Experiment Station for the financial support which made the study possible.

The writer wishes to recognize and thank the drafting department of the Agricultural Engineering staff for their assistance in preparing the tables and graphs presented.

TABLE OF CONTENTS

LIST OF TABLES

LIST OF FIGURES

Figure Page

CHAPTER I

INTRODUCTION

Forces due to dead loads and other gravity loads on structures may be easily accounted for, but in general, wind forces may not. Each year needless damage is done to farm structures because of the lack of information concerning wind loads or erroneous information.

Extensive tests have been conducted on the more "common" shapes of structures and the results have been used as a basis for building codes the world over. Haddon (1960) found that, in general, Codes of Practice are getting more realistic with respect to wind loading, but with the exception of the Swiss Building Code, he found none which considered a diagonal wind acting on the structure. In some of Haddon's investigations, he found the greatest pressure on roofs occurred when the roofs were subjected to diagonal winds. These findings point out the need for more complete investigation of the wind forces on structures.

The use of various configurations of concrete shell structures has rapidly been accepted by the American public in recent years. The hyperbolic paraboloid type of structure is highly desirable due to its "eye appeal", simplicity of structural action, and economical use of structural materials. Ease of construction and efficient design are inherent in that the formwork requires only straight generators and bending stresses in the concrete are minimized. All these factors combine to give a relatively low cost structure which is the reason for the rapid growth of

interest in hyperbolic paraboloid shells for light structural applications.

Information regarding the forces developed by wind loads on the shells must be available to the design engineer if failures are to be prevented. The nature of the hyperbolic paraboloid shell makes it possible for large roof areas to be supported on only one or two masts. Due to this fact, the need for information regarding the forces on the supports due to the wind is extremely critical for proper design. Because hyperbolic paraboloid shells are relatively new, little or no information is available concerning the forces induced by the wind.

Information on the effect of upwind barriers on wind flow characteristics is needed for more efficient and effective structural design. Certain investigators have noted induced oscillations or buffeting effects when upwind barriers were present. To date, most investigations involving buffeting effects have been made on two-dimensional bodies such as cylinders, plates or bluff objects. Such objects have in their wake a double row vortex system. Vertical solid barriers on a ground plane are believed to develop single row vortex systems. Exact characteristics of these systems are not known. Such vortex systems, when striking a structure, could cause failures due to overpressure on the surface on which the vortex acts.

This study was undertaken to determine the resultant forces and overturning moments acting on hyperbolic paraboloid shell models subjected to a one-dimensional flow pattern in a wind tunnel. In an attempt to conduct a definitive study and to limit the time required, only one configuration was tested and is illustrated in Figure 1. The force system was studied with the flow perpendicular to the two different sides of the shell.

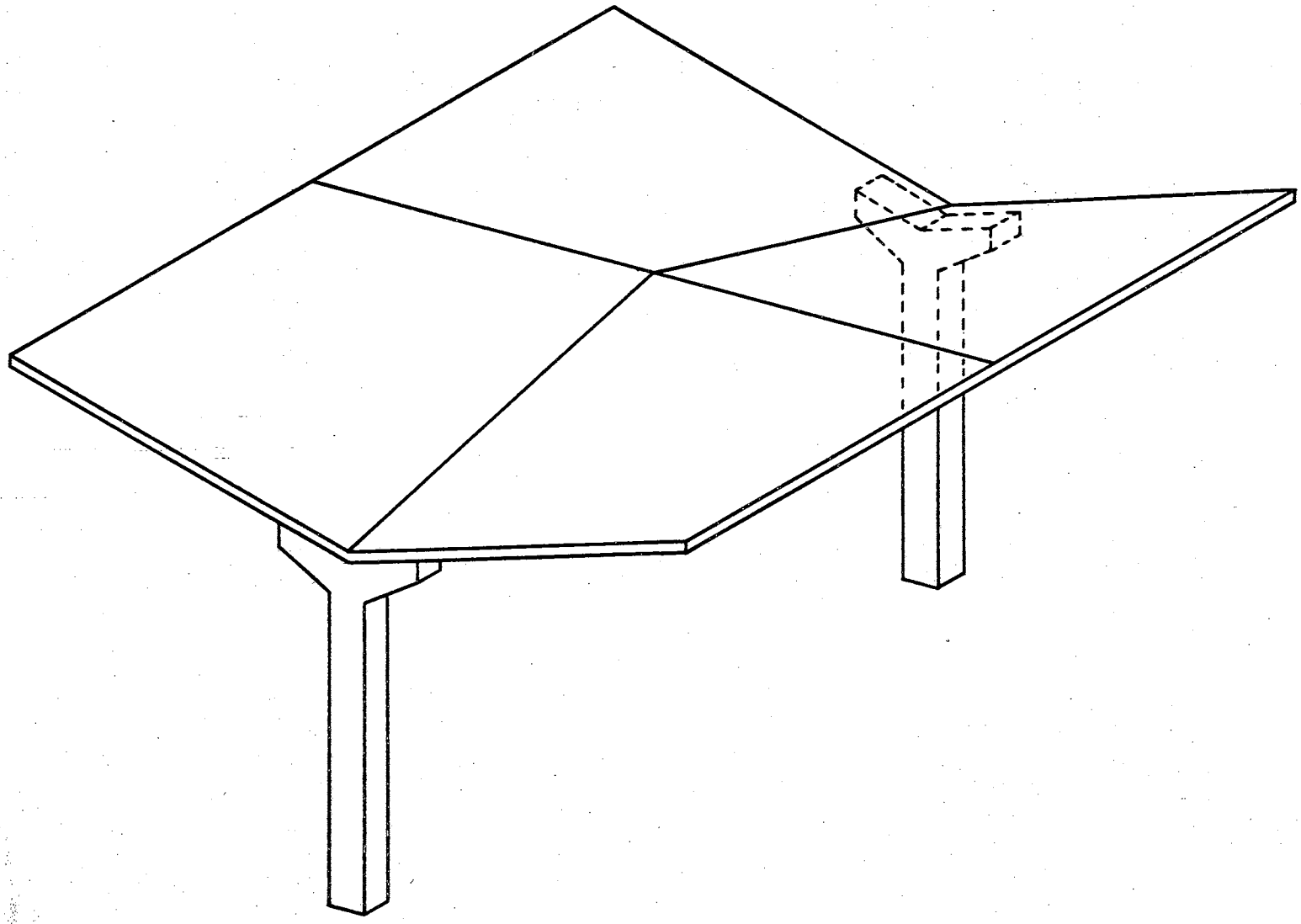

Figure 1: The Type of Hyperbolic Paraboloid Shell Configuration Used for the Experimental Investigation

CHAPTER II

REVIEW OF LITERATURE

Structure of the Wind

"The wind may be defined as motion of the air caused by gravity, by deflective forces due to the earth's rotation, and by centrifugal forces due to the curvature of the wind path." (Biggs, 1961).

Wind speed varies with height above ground. Numerous investigations have attempted to define this variation of profile. In general it has been found that the variation is dependent on a number of quantities, and is not necessarily the same at a given geographic location at all times. Also, there is a definite variation in the wind profile from one location to another.

Prandtl's (1952) development of a rational formula for the variation of velocity with height above a flat plane has been the basis for numerous investigations on this topic. Prandtl's development was based on an analysis of viscous shearing stresses in the boundary layer, and momentum transfer. It is based on the conservation of momentum theorem and assumes a two-dimensional flow, considered steady on the average. The final result was a general expression for variation of velocity with distance from the plane, for air of uniform density, in the form:

$$U = V^* \left(1/K \log \left[\gamma V^*/\nu\right] + C_1\right)$$

where, U = velocity at height Y,

V^* = $\sqrt{\tau/\rho N_e}$ = shearing stress velocity,

τ = shearing stress,

ρ = density of fluid,

K = L/Y,

L = mixing length,

C_1 = universal constant,

N_e = Newton's second law coefficient;

ν = kinematic visosity.

In regions of low turbulence, Prandtl found that velocity varied as the seventh root of the distance from the boundary if Reynolds' number was less than 10^5. He also concluded that the friction or boundary layer height from the surface increases as velocity increases. Prandtl's expression for wind speed as a function of height when turbulent flow predominates was:

$$U = V^* (5.75 \log Z/K + C_2)$$

where, U = wind velocity at height Z,

Z = height above the ground,

C_2 = universal constant which varies between 5.0 and 8.5,

K = height of irregularities such as houses and vegetation,

V^* = shearing stress velocity.

Several investigators preferred the use of a so called "power law" expression to describe the wind profile. The general form of the power law equation is:

$$V_2 = V_1 (Z_2/Z_1)^{\alpha}$$

where, V_2 = velocity at height Z_2,

V_1 = velocity at some reference height Z_1,

α = an exponent, to be determined from observations.

The value of "α" has been investigated by many researchers and large variations in its value are noted. Most variations are due to the characteristics of the site where observations were recorded. The presence of natural barriers as well as other structures influences the flow pattern and shape of the velocity profile.

Geiger (1950) found that α decreased with increasing height. He found that near the ground, (within 1-½ meters), α could be considered constant but varied with temperature. He concluded it was impossible to separate the effects of temperature and the effects of wind gradient.

Sutton (1953) studied diurinal variations at heights from three to thirteen meters and found $\alpha = 0.13$. He also presented Prandtl's equation for completely rough flow as:

$$U/V^* = 1/K \ln Z/Z_o$$

where, $V^* = \sqrt{\tau/\rho N_e}$ = friction velocity,

Z_o = roughness length,

K = Karman's constant,

N_e = Newton's second law coefficient;

U = velocity at height Z.

Sherlock (1952) studied wind velocities from 0 to 250 ft. elevations during storms and found $\alpha = 1/7$.

Pagon (1953) concluded that $\alpha = 0.167$.

Brooks (1959) concluded from his investigations that wind velocity profile expressions, such as the power law, are only time averages of erratic instantaneous distributions which are too complicated to use.

From this brief explanation of the structure of the wind and wind profile, it is evident that a person requiring exact knowledge of the wind profile must investigate it at the location at which such information is needed. Others may select one of the many exponents for the power law equation, which have been found, or use another method such as Prandtl's rational derivation, or select a method of his own which he feels will best describe the profile for his particular application.

The Use of Weather Data in Structural Design

Voluminous records of wind velocity have been taken by first order stations of the United States Weather Bureau and compiled for use in determining the maximum wind speed to be expected in practically all areas of the United States. The data are not comparable due to the varying location of recording stations. Attempts to unify the data have been made by Thom (1960) Chief Climatologist of the United States Weather Bureau. Thom's presentations consist of contour maps showing the fastest mile of wind for a given probability of occurrence adjusted to a height of 30 ft. Teter, Neubauer, and Pedersen (1963), in cooperation with the American Society of Civil Engineers, have developed maps for the 10 and 25 year recurrence interval, extreme-mile winds similar to the 2, 50 and 100 year maps by Thom. They felt such maps were necessary in view of the rapid rate of obsolesence and low hazard to human life involved in farm buildings.

Wind forces on structures are usually only of concern during storms. The type of storm for which observations are taken play an important role in the interpretation of the observation. Extratropical storms, hurricanes

(both mature and decaying), and tornadoes all possess different wind profile characteristics and should be analyzed differently.

Localized high wind velocities lasting for a short interval are known as gusts and also possess characteristics which should be taken into consideration in the selection of a design wind velocity. Durst (1959) states that the critical time during which a gust affects a member is usually of the order of 15 seconds or less.

Sherlock suggested the use of a gust factor for determination of design speed. The design wind speed would be equal to the highest "five-minute velocity" multiplied by the gust factor. He related gust factors by the following equation:

$$F_z = F_{30} \, (30/z)^{.0625}$$

where, F_z = gust factor at height z,

F_{30} = gust factor at height of 30 ft.

The maximum wind speed which a structure will encounter during its life is seen to be dependent on several factors and the methods vary for determining this critical speed. Each engineer must satisfy himself with the results of some particular method and proceed on that basis.

Wind Force Coefficients

After selecting a design wind speed, the design engineer needs to be able to predict the forces on the structure which would result if the design wind speed occurred. To do this, coefficients have been defined to predict the horizontal and vertical forces acting on an object due to air flow about that object.

Wind possesses kinetic energy because of the velocity and mass of the moving air. Obstacles in the path of wind cause transformations from

kinetic energy to potential energy in the form of pressure. The intensity of pressure is dependent on the shape of the obstacle, angle of incidence of the wind, velocity and density of the air.

The horizontal force parallel to the wind is usually expressed by the equation:

$$\text{Drag} = C_D \; q \; A$$

where, C_D = drag coefficient,

q = dynamic pressure, $\frac{1}{2} \rho \, N_e V^2$;

A = horizontally projected area of the object.

Similarily the vertical lift coefficient is expressed:

$$\text{Lift} = C_L \; q \; A$$

where, C_L = lift coefficient;

A = vertical projected area.

Values for the coefficients must be experimentally determined. The magnitude of the coefficients has been found to depend on (1) the geometrical shape, (2) orientation of the object in the wind stream, (3) roughness of the surface, (4) the size of the object, and (5) the velocity of the wind stream.

Pressure coefficients are used to describe the local pressure at any point on the surface of a building.

$$P = C_p \; q$$

where, P = local pressure,

C_p = pressure coefficinet,

q = dynamic pressure.

Pressure coefficients must be determined experimentally and are necessarily dependent on the same variables which effect force coefficients.

Openings in structures cause large changes in the pressure coefficients by causing the development of internal wind pressures which may be of considerable magnitude if the openings are large.

Pressure coefficients for common building types and typical proportions have been determined and are available for design use. Different sources many times do not give the same values for similar shaped structures indicating the complexity of the problem. Biggs, (1961) and the American Society of Civil Engineers Committee on Wind Forces felt that the Swiss Building Code was probably the most accurate source of information on pressure coefficients.

Experimental Techniques

Haddon (1960) states that in the light of the discrepancies encountered from different sources of information regarding the results of wind tunnel tests, it is necessary to determine a system of testing which will give accurate results so that tests on scale models may be used to determine the wind loading of the prototype structure. His list of sources of error in testing procedure includes:

1. Scale effect, i.e.; change in Reynolds' number.
2. Surface of the ground and velocity gradient.
3. Method of mounting model.
4. Relation of model size to tunnel size.

Reynolds' number was first used by Osborne Reynolds during his investigation of fluid motion in tubes and is defined as:

$$\text{Reynolds' number} = VL\rho N_e/\mu$$

where, V = fluid velocity,

L = linear dimension of the object,

ρ = density of fluid,

μ = viscosity of fluid,

N_e = Newton's second law coefficient.

Reynolds found that if the flow about geometrically similar objects was to be similar, the value of Reynolds' number must be the same. This requirement has largely been ignored in applying the results from wind-tunnel tests of sharp or bluff edged objects to full scale structures. Attempts in which correlation with full scale models have been attempted tend to confirm this practice. Irminger and Nøkkentved (1936) found Reynolds' number did affect the pressure distribution on sharp edged bodies in their tests and attributed the effect to the windward ground friction which created a windward vortex region.

Other investigators have differing opinions as to the effect of Reynolds' number. Van Erp (1950) refers to the work of Eiffel and concludes there was no scale effect and that Reynolds' number was one when pressure distributions were transferred to larger scale structures. Castleman and Mirsky (1951) feel the absence of scale effect is equivalent to zero viscosity. Thus, Reynolds' number would be infinitely large. The present writer is not in agreement with either of these views. Reynolds' number need not take on any one particular value for scale-effect to be absent. If scale-effect is absent, within a certain range Reynolds' number may take on any value in that range and not change the drag or lift coefficient which is determined, regardless of the size object involved. The diversity of opinion is large and it appears that each particular structural configuration warrants study concerning scale effect.

Bridgman (1931) approached the problem of scale effect as follows. For models tested in air, $\rho N_e/\mu$ is essentially constant. Therefore, the product of (V)(L) must be constant for model and prototype to conform to the theories of similitude, Murphy (1950). It is impractical, if not impossible, to achieve model studies of this nature, due to the high velocities which are required. Bridgman found that by dividing the value of the resistances found for the model by V^2L^2/ρ, at high values of wind velocity, the function will approach a constant value asymptotically. Thus tests conducted with wind velocities near the constant value should be valid for application to other geometrically similar objects.

To have accurate correlation between model and full scale buildings, the velocity gradient in the tunnel should be known and ideally would be similar to that of nature, taking into account scale factors. Rice (1961) obtained a velocity profile which was described by the power law equation with value of $\alpha = 1/4$. This was accomplished by spacing rods of different diameters at various heights above the wind tunnel floor.

To obtain correlation with prototype conditions, it is generally agreed that models should be mounted on the floor of an enclosed tunnel. Mounting above the floor of the tunnel in an attempt to eliminate the velocity gradient is undesirable, as previously discussed, and tends to give unrealistic results.

Friesen (1962) states that models should not take up more than five or six percent of the wind tunnel area to prevent blockage effects. Haddon (1960) lists the allowable height or width of a model as 15% of tunnel height or width to prevent the effect of tunnel interference. Tunnel effects or blockage effects are due to the fact that the air-stream is

deflected upwards by the model. The deflection decreases with height for a distance of about ten times the model height. Deflection of the air-stream is then no longer evident.

Data concerned with wind effects on structures have usually been obtained by measuring the static pressure at small peizometer holes at various locations in the surface of the models being tested. This method is quite slow and tedious and does not yield readily an expression for the total force on the structure. Nelson and Giese (1962) developed a load-weighing system which enabled the determination of wind-force reactions directly on the component surface. Each of the corners of the roof section or wall surface was supported by special reaction weighing bars. The bars were mounted on the outside of the testing channel and arranged to respond only to reactions normal to the plane of the roof or wall surface.

The ideal test procedure would be one such that the investigator could determine the total force system acting on the model for a given wind speed and direction. A resultant force system, including horizontal and vertical forces as well as the overturning moments, could then be determined.

Barriers, Oscillations and Buffeting Effects

The pressures of forces on a structure immersed in a wind stream result from changes in velocity around the structure. Determination of wind forces is in reality a transient force problem. However for purposes of structural design, in most cases it is sufficiently accurate to consider that these forces are steady. Even in using such an approach the engineer should be cognizant of the transient forces involved. In instances where unsteady velocities or alternating forces resulting from periodic vortex formation are present, the time variation of force must be considered.

Horner (1958) states a "double-row vortex trail" or "vortex street" is found in the wake of two-dimensional bodies such as cylinders, plates or bluff rods. The number of vortices formed at one side of the street is presented by the so-called Strouhal number:

$$S = FH/V$$

where, H = height or thickness of body producing the street,

F = frequency of vortex formation,

V = flow speed between body and fluid.

Oscillations of considerable magnitude can be excited by comparatively small aerodynamic forces if the frequency of the vortex street and lateral forces come into resonance with the natural bending frequency of the structure.

Wind excited oscillations of a 150 ft. high steel stack with a diameter = 4 ft., are reported by Scruton (1955) beginning at a speed corresponding to a Strouhal number = 0.2. The oscillations continued up to twice the speed at which they first started, dangerously shaking the structure. Price (1956) investigated the effect of a shroud about a circular cylindrical member. It was effective in suppressing vortex excitation at subcritical, transitional, and supercritical values of Reynolds' number. The transitional Reynolds' number was defined as the value at which a radical reduction in the drag coefficient occurred with increasing Reynolds' number.

Haddon reports that a wall, 10 ft. high and 60 ft. windward from a 20 ft. high shed with 30 degree roof slope will, assuming normal flow, change the average wind pressure from approximately zero to $0.3P_s$, where

P_s = stagnation pressure. The same wall with diagonal flow was reported to increase suction to as much as $3.0P_s$.

Nelson (1957) and Rice (1961) also noted strong oscillatory forces on structures in the wake of sharp-edged vertical barriers on a ground plane.

The A.S.C.E. Task Committee, (Biggs, 1961), on wind forces states that the buffeting action due to oscillations induced in the wake of an obstruction is generally irregular, resulting in short bursts of amplitude and has rarely been catastrophic. This statement seems questionable in the light of the above mentioned observations and indicates the need for more research dealing with upwind-barriers and their effects.

CHAPTER III

THE EXPERIMENTAL STUDY

Objectives

The objectives of this experimental investigation were:

1. To determine the horizontal, vertical, and overturning forces acting on a hyperbolic paraboloid shell structure due to wind loads.

2. To determine the effects of variation of Reynolds' number on the forces acting on the shell.

3. To develop a direct method of measuring the resultant wind force components acting on a model during wind tunnel tests.

Experimental Design

Similitude Requirements

The results of the experimental investigation were intended to be applicable to geometrically similar structures; therefore the design of the experiment was carried out according to the principles of similitude as described by Murphy (1950). The quantities which were felt to be pertinent to this investigation are listed and illustrated in Figure 2.

The width and projected height of the shell were included as pertinent quantities because these factors completely define the shape of the shell. The shape of an object determines the flow pattern about the object and thus the forces acting on it. The height of the support is a measure of the height of the shell above the ground plane. If the shell were constructed close to the ground, interference of the flow beneath the shell would possibly occur.

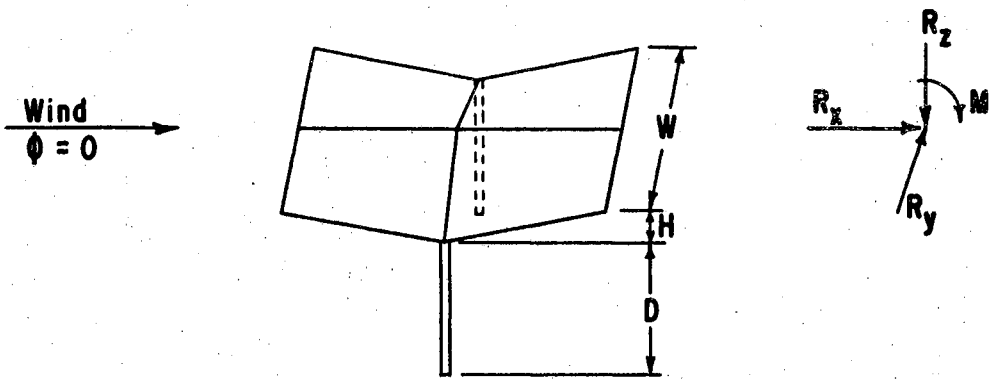

PERTINENT QUANTITIES

No.	Symbol	Description	Dimensional Symbol
1	W	Width & Length Of Shell	L
2	H	Projected Height Of Shell	L
3	D	Height Of Support	L
4	R_x	Resultant Force, X Direction	F
5	R_y	Resultant Force , Y Direction	F
6	R_z	Resultant Vertical Force	F
7	M	Resultant Overturning Moment	FL
8	V	Wind Speed	LT^{-1}
9	ρ	Density Of Air	ML^{-3}
10	μ	Viscosity Of Air	FTL^{-2}
11	N	Newton's Second Law Coefficient	$FM^{-1}L^{-1}T^{2}$
12	ϕ	Wind Direction	

Figure 2: Definition Sketch of the Shell Model and Pertinent Quantities

The velocity and physical properties of the air, i.e., density and viscosity, were also included, so that the effect of Reynolds' number could be evaluated.

Changing the direction of the impinging wind would alter the flow characteristics about the shell; therefore the wind direction, $\emptyset$, was included as a pertinent variable. The designation of the tests with wind flow perpendicular to the horizontal edge was $\emptyset$=0, thus tests with flow perpendicular to the V-shaped edge were designated $\emptyset$=90.

The pertinent quantities were then combined according to the Buckingham Pi Theorem to form the dimensionless parameters listed in Table I.

The force system was evaluated as influenced by the rise to width ratio of the shell as well as the height of the shell above the ground plane. The selection of the values to be used for the slope and height parameters were made in accordance with the general practice in full-scale shells. For a given shell width, W, the strength increases with height, H. A value of H/W = 1/8 gives an efficient design for shells of about 40 ft. width. Because minimum shell thickness is generally determined by the amount of concrete necessary for weather protection of the steel reinforcement, a shell of less width might easily have an H/W ratio of less than 1/8. The values selected for H/W were 1/6, 1/8, 1/10, and 1/12. The extreme values of the height parameter, 0.2 and 0.5, are equivalent to a 40 ft. wide shell at a height of 8 ft. and a 20 ft. shell at 10 ft. height respectively.

Testing Schedule

The size of the models tested was selected to be 2 ft. square, thus the height, H, was 4 in., 3 in., 2.4 in., and 2 in. corresponding to π_6 values of 1/6, 1/8, 1/10, and 1/12 respectively. The height above the

TABLE I
DIMENSIONLESS PARAMETERS FORMED FROM THE PERTINENT QUANTITIES

No.	Term	Description	Symbol	Values
Π_1	$\frac{R_X}{N_e H W \rho V^2}$	Drag Parameter, X Direction	C_X	Dependent
Π_2	$\frac{R_Y}{N_e H W \rho V^2}$	Drag Parameter, Y Direction	C_Y	Dependent
Π_3	$\frac{R_Z}{N_e H W \rho V^2}$	Lift Parameter	C_Z	Dependent
Π_4	$\frac{M}{N_e H W^2 \rho V^2}$	Overturning Moment Parameter	M_O	Dependent
Π_5	$\frac{V W \rho N_e}{\mu}$	Reynolds' Number	R_N	———
Π_6	$\frac{H}{W}$	Slope Parameter	—	1/6, 1/8, 1/10, 1/12
Π_7	$\frac{D}{W}$	Height Parameter	—	0.2, 0.3, 0.4, 0.5
Π_8	ϕ	Wind Direction	ϕ	0°, 90°

tunnel floor, D, ranged from 4.8 in. to 12.0 in. The schedule of tests was set up to vary each of the independent π terms through its selected values while holding the other constant. The combination of the parameters and values of the pertinent quantities for each of the tests are given in Table II.

TABLE II
PARAMETER COMBINATIONS

Run	H/W	D/W	H (in.)	D (in.)
1	1/6	.30	4.0	7.2
2	1/10		2.4	
3	1/12		2.0	
4	1/8		3.0	
5		.20		4.8
6		.40		9.6
7		.50		12.0

This schedule of parameter combinations was carried out for both directions of flow over the shell, i.e., $\emptyset$=0 and $\emptyset$=90.

Another schedule of tests was set up to determine the effects of a solid upwind barrier of height B, at a distance S from the shell. For these tests B and S must be included as pertinent quantities thus two new π terms are required. They are π_7 = B/D and π_8 = S/D. Since severe oscillatory forces made it impossible for all the tests to be completed, the schedule is not presented here but is discussed in the chapter concerning test results.

CHAPTER IV

EQUIPMENT

Force Sensing Devices

The Theoretical System

The requirements of the support system designed to measure the forces acting on the model were stability and statical determinacy. A system having three supports was selected with two force components at each support. The three supports were designated A, B, and C with the direction perpendicular to the horizontal edge of the model and in a horizontal plane designated X, the direction 90 degrees from X, designated Y and the vertical direction Z. The resultant forces and moment were expressed acting at the top and center of the shell. Figure 3 is a sketch of the system showing the coordinate system and location of the measured and resultant forces. The resultant forces are designated by "R" with a subscript denoting their direction while the measured forces are designated by an "F" with two subscripts. The first subscript denotes the place of measurement, i.e., support A, B, or C, and the second designates their direction.

Six equations of statics are available for the solution of the system. They are: the summation of forces in each direction equal zero and the summation of moments in each of the three planes equal zero. The overturning moment, M, is in the X, Z plane when $\emptyset$=0 and the Y, Z plane when $\emptyset$=90. Table III lists the equations of statics used and the resultant force and moment equations.

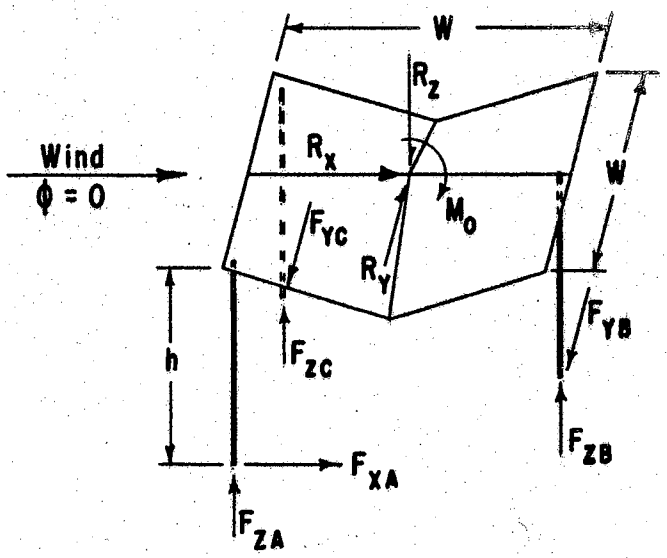

Figure 3: The Theoretical Force System

TABLE III
SOLUTION OF THE RESULTANT FORCE SYSTEM

Equation Of Statics		Resultant Equations
$\Sigma F_X = 0$		$R_X = -F_{XA}$
$\Sigma F_Y = 0$		$R_Y = F_{YB} + F_{YC}$
$\Sigma F_Z = 0$		$R_Z = F_{ZA} + F_{ZB} + F_{ZC}$
$\Sigma M_{(X,Z)} = 0$	When $\phi = 0$	$M_O = F_{XA}(h) + (F_{ZB} - F_{ZA} - F_{ZC})(W/2)$
$\Sigma M_{(Y,Z)} = 0$	When $\phi = 90$	$M_O = (F_{ZC} - F_{ZA})(W/2) - (F_{YB} + F_{YC})(h)$

The Physical System

The three supports for the shell models were made of 5/8 inch outside diameter steel tubing and 3/8 inch diameter tubing which could slide within the larger tubing giving a means for adjusting the height of the model. To fix the model at the desired height two set screws were used running through the larger tubing and clamping on the smaller. Round supports were used to reduce the amount of interference of the flow pattern beneath the shell. The supports were long enough to pass through the floor of the wind tunnel thus eliminating force sensing equipment from the wind flow pattern.

To measure the forces at the lower end of the supports in only two directions required the development of a system of "weighing bars." The weighing bars were designed so that the forces in two perpendicular directions, one vertical and one horizontal, could be determined. Figures 4 and 5 illustrate various characteristics of one of the weighing bars. Two pairs of electrical resistance strain gages were attached as shown such that any applied force in the plane of the two forces to be determined would cause strain in one or both of the gage pairs depending on the direction of the applied load. The connection between the end of the weighing bar and the support was a ball joint to minimize torque transmission to the weighing bars. Torsional resistance at the end of any of the three bars would have removed the statical determinacy of the system. Also, torsional loads would have induced strain in the various gage pairs which would have been interpreted as an applied load. The longitudinal axis of the bar was perpendicular to the plane formed by the forces to be determined. The base end of the bar was supported by ball bushings to minimize the longitudinal force being resisted simulating a frictionless condition. This prevented

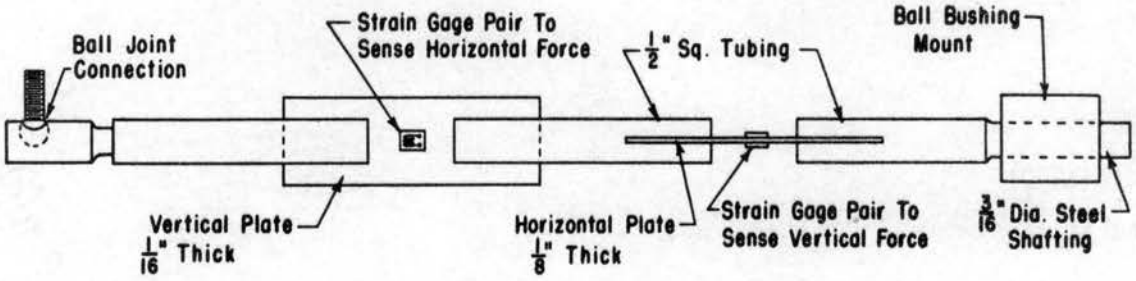

Figure 4: Sketch of a Force Sensing Weighing Bar

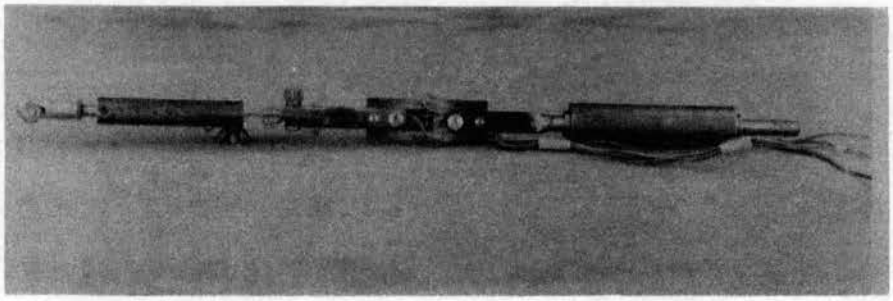

Figure 5: Plan View of an Assembled Weighing Bar

axial stresses from being developed which would have caused an unwanted strain indication. The ball bushings were mounted on a frame work fastened to the floor beneath the wind tunnel. The frame work was pivoted above a vertical axis passing through the center of the model thus allowing rotation of the system to change the direction of the impinging wind. Figure 6 shows the supports and force sensing equipment with the shell model in place.

The thickness of the flat plates on which the strain gages were mounted was selected to provide sensitivity to the lighest expected load yet limit the deflection to 1/2 inch in either direction for maximum expected load. The maximum and minimum loads were calculated by assuming the lift and drag coefficients, C_L and C_D, to vary from 1.0 to 0.1 for the range of velocities at which the tests would be conducted.

A "Sanborn" Dual Channel Carrier-Amplifier Recorder was used as the strain signal amplifying and recording device. This made it possible for the load indication from both gage pairs of one particular weighing bar to be recorded simultaneously.

The weighing bars were calibrated by loading them in each direction with loads of known magnitude and recording the strain reading as units of deflection on the recorder chart. The relationship between applied load and units deflection was linear. The slope of the relationship was determined by a linear regression analysis for each weighing bar in each of the directions. All bars were checked carefully to be sure that applied load in either direction did not cause a false strain indication, e.g., load in the horizontal direction did not cause strain in the gage pair for sensing the vertical force.

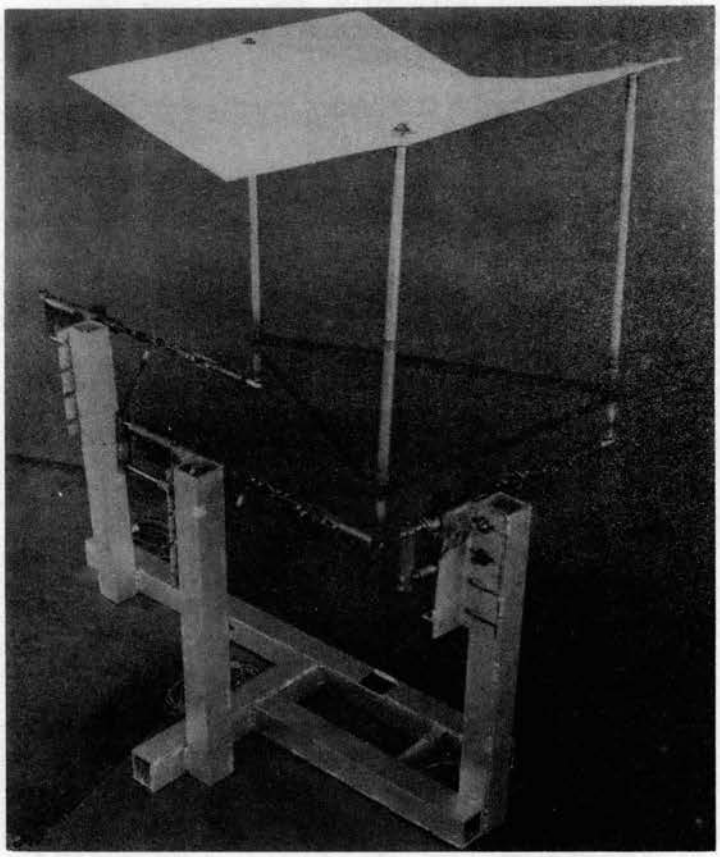

Figure 6: The Complete Force Sensing System with Shell Model in Place

Shell Models

To obtain a true hyperbolic paraboloid shell configuration, a material for constructing the models was needed which could be easily formed. Another desirable characteristic for the model material was light weight yet adequate rigidity to prevent excessive deformation under action of the wind. Fiberglass was selected. To form the fiberglass shell models, plaster of paris molds were poured to generate the desired shape. Each of the four quadrants was made by the use of the plywood box form illustrated in Figures 7 and 8. The molds having the most slope were poured first. After the quadrants were cast they were fastened together as shown in Figure 9 and the fiberglass applied. Fiberglass cloth and resin were used alternately until a shell about 3/32 inch thick was formed. The model was then sanded to smooth any roughness present on the surface and edges. The sides of the plywood box form were then changed to correspond to the model with the next slope, the plaster of paris quadrant placed in the box and a new hyperbolic paraboloid quadrant formed. This process was continued until all four models were complete. Figure 10 shows one of the finished shell models.

Wind Tunnel

General Characteristics

The agricultural engineering wind tunnel at Oklahoma State University was used for the study. The tunnel was designed for low speed testing. It is an open return, induced flow type, 50 ft. in length having a four ft. square cross-section. The axial flow blower is 60 inches in diameter and consists of 16 adjustable pitch blades. The blower is powered through a variable speed belt drive connected to a 15 hp. electric motor. A piezometer

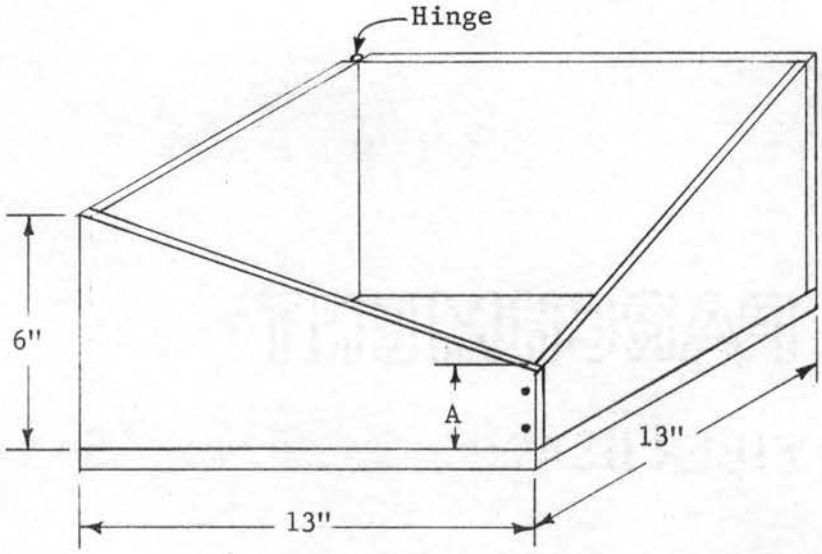

A
2"
3"
3.6"
4"

Figure 7: Sketch of Plywood Box Form Used for Making Plaster of Paris Molds

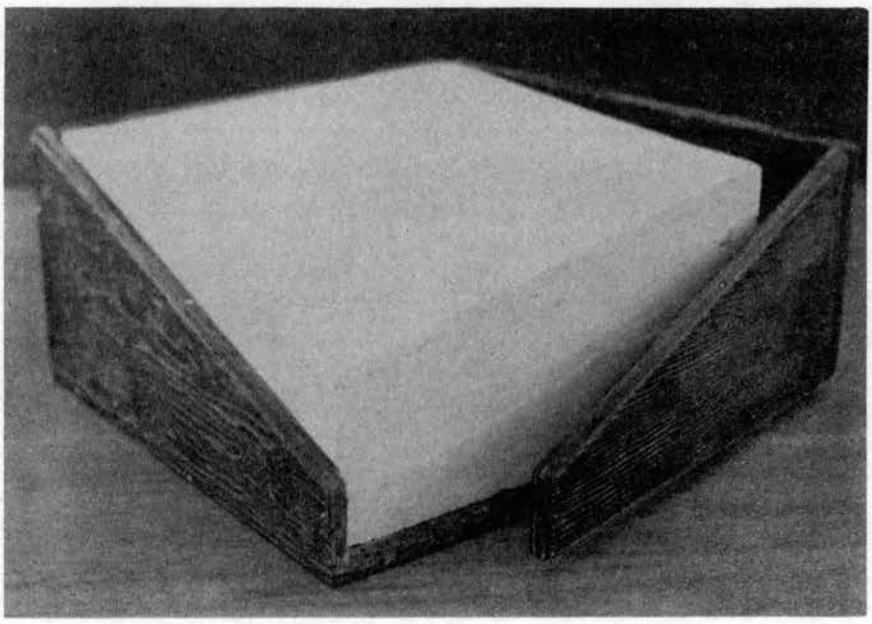

Figure 8: Plywood Box Form with Plaster of Paris Mold

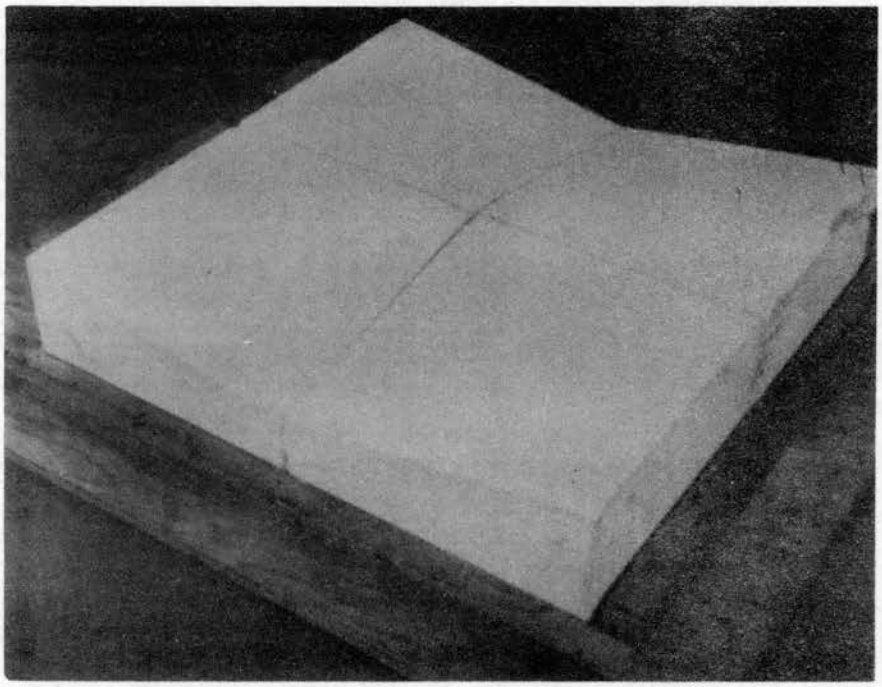

Figure 9: Mold Ready for the Application of Fiberglass

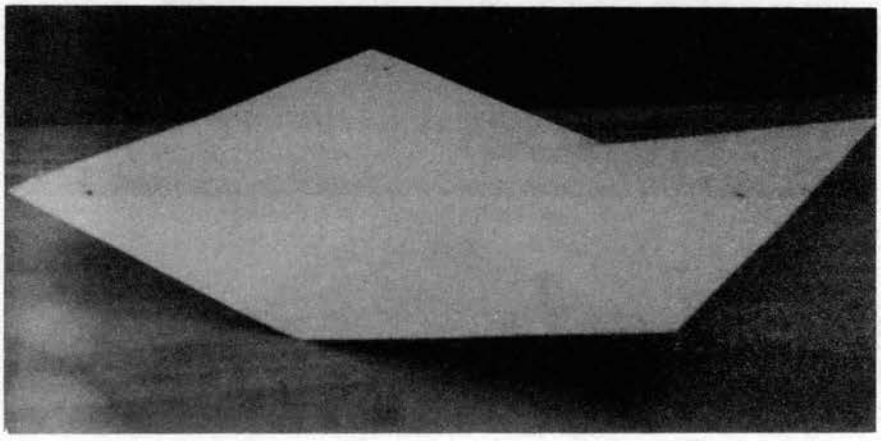

Figure 10: Hyperbolic Paraboloid Model

ring is located near the exhaust section of the wind tunnel to allow measurement of static pressures by the use of a precision manometer. The air passing through the tunnel was recirculated to provide minimum changes in the properties of the air during testing. Figure 11 shows the arrangement and dimensions of the wind tunnel.

Velocity Determination

To determine the variation of velocity in the wind tunnel a velocity traverse was made with a pitot-static tube at 64 points on a 6 inch grid within the tunnel. Traverses were made for four different wind speeds. The piezometer ring static pressure was recorded for each speed as well as the velocity head. The velocity was essentially constant for all locations, with the exception of reduced velocity in the corners and a slight increase in velocity with height.

To determine the velocity of the wind, acting on the model, by reading the piezometer ring static pressure, the following procedure was used:

1. The area in the tunnel which the model would occupy was determined. Eight points from the velocity traverse were within the area.
2. The slope of the Velocity Head, h_A, vs. Piezometer Static Pressure, H, curve was determined by a linear regression analysis for each of the eight points. The average value of the equation for the linear relation was:

$$h_A = 0.799\ H$$

where, h_A = velocity head, (in. of methanol);

H = static head, (in. of water).

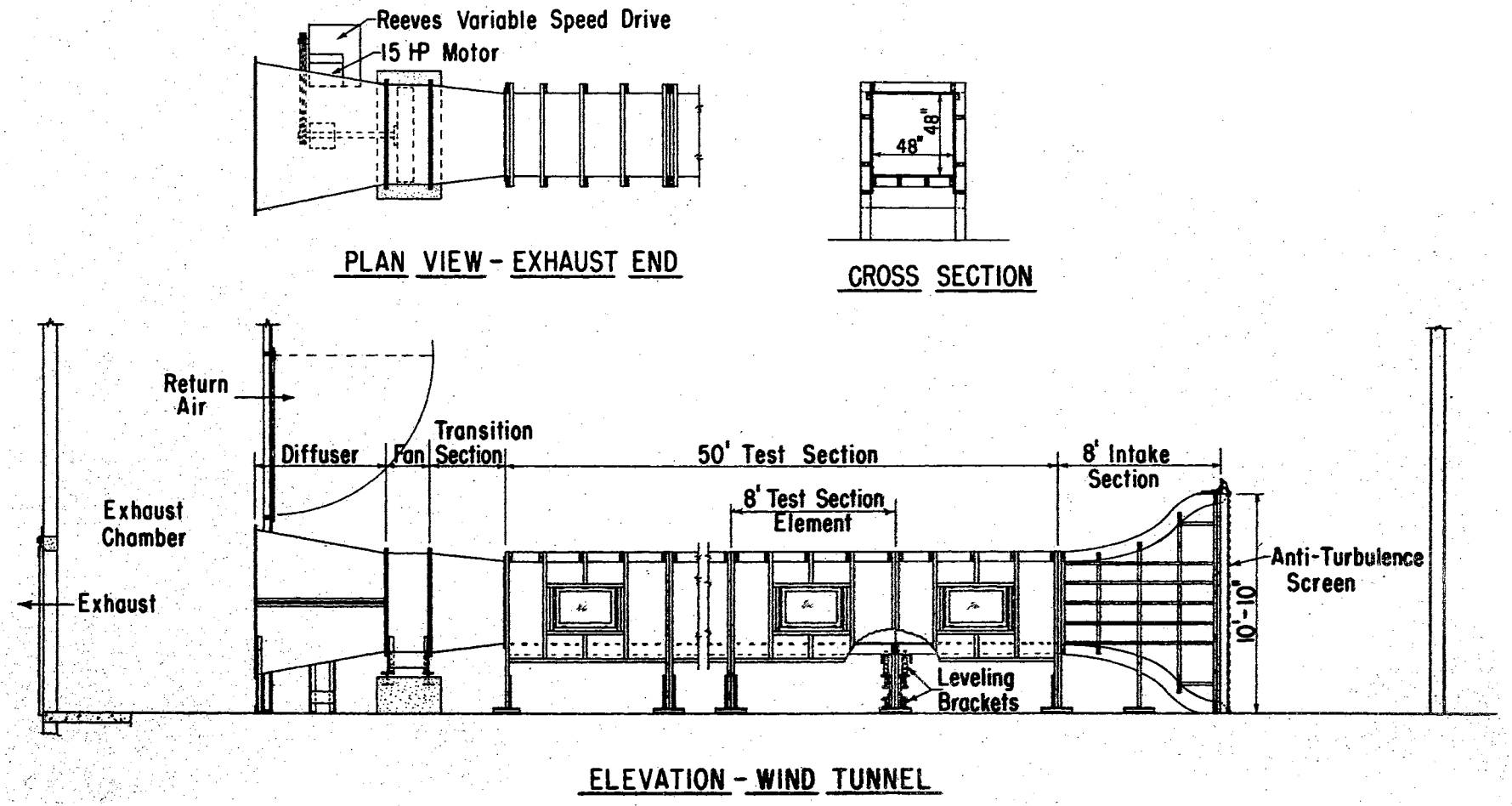

Figure 11. The Agricultural Engineering Research Wind Tunnel.

3. Velocity = $\sqrt{2g\,H_a}$

where, $g = 32.2$ ft/sec^2;

H_a = velocity head, (ft. of air).

but, $H_a = h_A\ \rho_A/12\ \rho_a = (.799\ H)\ \rho_A/12\ \rho_a$

where, ρ_A = density of methanol, (49.38 16/ft^3);

ρ_a = density of air.

then, velocity = $2(32.2)(.799\ H)(49.38)/12\ \rho_a$

$= 14.55\ H/\ \rho_a$

A "Bristol" Thermo-Humidigraph was used to record the laboratory temperature and relative humidity during testing. This instrument was checked each day of testing by the use of a sling psychrometer to insure proper calibration. During the tests the temperature within the tunnel was recorded. The density of the air was then determined by the use of a psychrometric chart assuming the air at the same moisture content in the tunnel as in the laboratory space.

CHAPTER V

PROCEDURE

The following procedure was followed in setting up and conducting the experiments:

1. The temperature and relative humidity recording device was calibrated by the use of a sling psychrometer.
2. The correct shell model was selected for the run to be conducted and then mounted on the supporting masts.
3. The height of the model above the tunnel floor was set.
4. The force sensing equipment was visually checked for proper alignment; then lubricated to minimize friction effects.
5. The recorder was adjusted to give a zero load indication for each of the six force components.
6. The "Run" was then conducted at a minimum of five different wind speeds. The wind speed varied from approximately 24 to 45 miles per hour with some tests begun at about 10 miles per hour. For each wind speed, the static pressure at the piezometer ring was recorded and traces from the recorder were made for each of the six strain gage pairs. The laboratory temperature, relative humidity, tunnel temperature, and barometric pressure were recorded at the beginning and end of the test run.
7. Steps 4-6 were then repeated twice to give a minimum of three replications for each test run.

From the data obtained in the laboratory the magnitude of the measured forces was calculated. The velocity was calculated by the use of the procedure described in the previous section on velocity determination. The resultant forces and overturning moment were determined. Values of the dependent π terms were calculated and recorded. The average value of the dependent π terms for the three replications was computed for analysis and discussion of results.

The values of the six measured forces and the relative velocity, ρV^2, are shown in the appendix for tests conducted without an upwind barrier.

CHAPTER VI

PRESENTATION OF DATA

Interpretation of the Dependent Pi Terms

The dependent pi terms, $\pi_1 = C_x$, and $\pi_2 = C_y$, are drag coefficients. Their relationship to the drag coefficient, C_D, of the usual drag equation; Drag = C_D q A, may be determined as follows:

$$\pi_1 = C_x = R_x/N_e HW\rho V^2 \text{ or } R_x = C_x N_e HW\rho V^2$$

where, R_x = drag when $\emptyset$=0,

q = dynamic pressure = $\frac{1}{2}\rho N_e V^2$

therefore,
$$\tfrac{1}{2}C_D N_e A\rho V^2 = C_x N_e HW\rho V^2$$
$$A(C_D/2) = C_x HW$$

The area, A, projected horizontally onto a vertical plane for a hyperbolic paraboloid shell is HW/2.

Then,
$$C_x = C_D/4$$

A similar relationship may be developed between $\pi_3 = C_z$, and the lift coefficient, C_L of the equation; Lift = C_L q A. In this case A is the area of the shell projected vertically onto a horizontal plane. The solution then involves the use of π_6 = H/W, and is:

$$C_z = C_L/\ 2\ \pi_6$$

$\pi_4 = M_o$, the dependent pi term involving the overturning moment is then a moment coefficient.

The objective of the study was then to determine these dimensionless coefficients, which describe the force system acting on the shell structure as affected by changes in:

1. Reynolds' number, π_5
2. Slope parameter, π_6
3. Height parameter, π_7
4. Direction of the wind, π_8

Reynolds' Number Effects

For most sharp-edged objects it has been determined that the drag and lift coefficients are not affected by changes in Reynolds' number. The hyperbolic paraboloid was expected to exhibit such characteristics. To determine if such was the case, graphs of the dependent π terms and Reynolds' number were plotted and are presented in Figures 12 through 18. In some cases the coefficients were found to be dependent on Reynolds' number, R_N, for the range in which the tests were conducted. The range of R_N for the tests varied from approximately 1.5×10^5 to 7.5×10^5.

$\phi=0$

The drag and lift coefficients were notably dependent on changes in Reynolds' number. The maximum observed values were approximately 1.5 to 2.0 times greater than the minimum. Both coefficients showed a peak value at about $R_N = 4 \times 10^5$ and then decreased with increasing Reynolds' number. The positive value of the lift coefficient, C_z, indicates the resultant vertical force on the shell model was in a downward direction. The moment coefficient, M_o, was minimum at $R_N = 5.5 \times 10^5$ for one test. All other runs showed the moment coefficient to be increasing with increasing Reynolds' number. The range of observed coefficients was from 0.13 to 0.36.

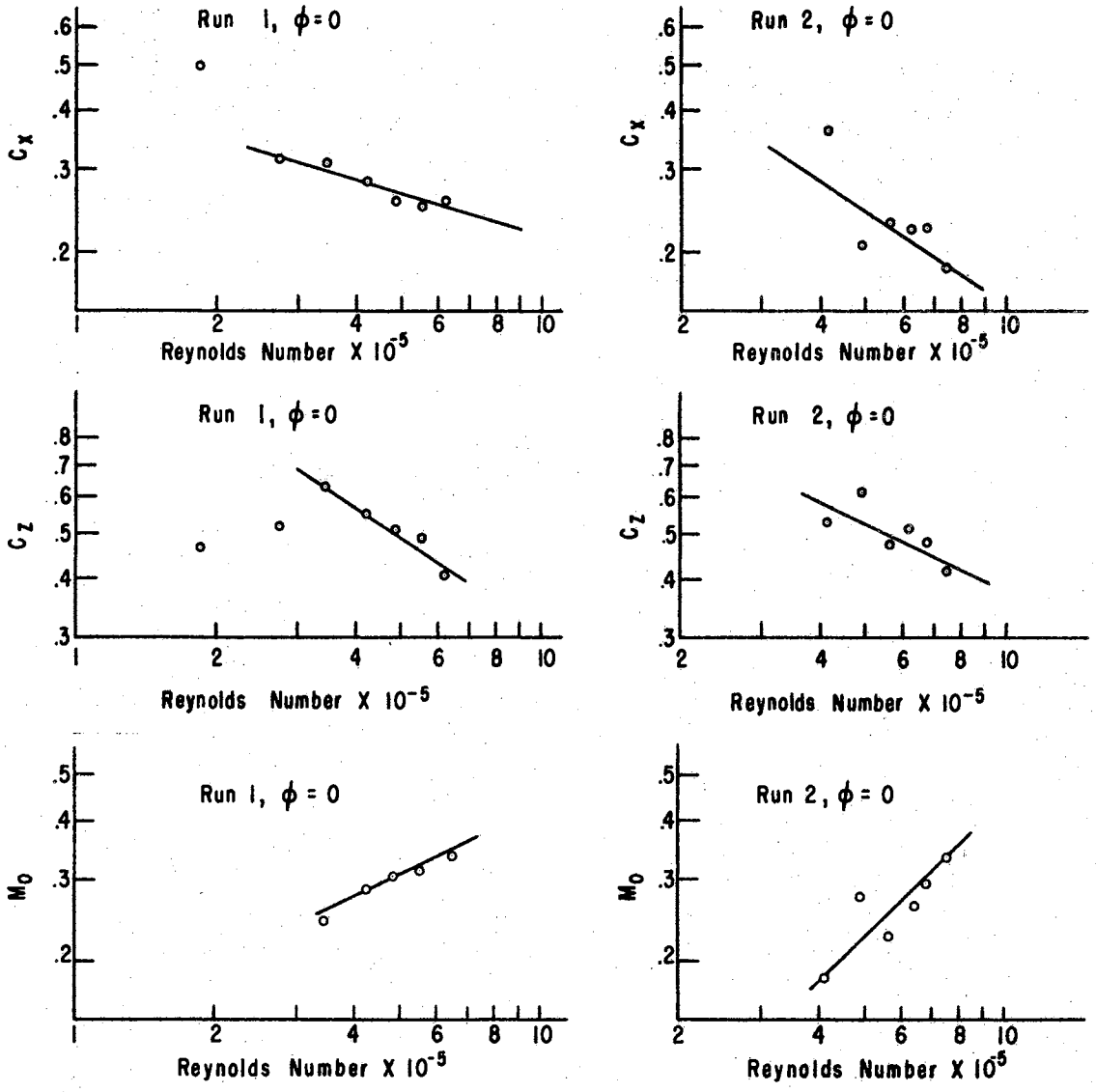

Figure 12: Effect of Reynolds' Number for Run 1 and Run 2, Ø=0

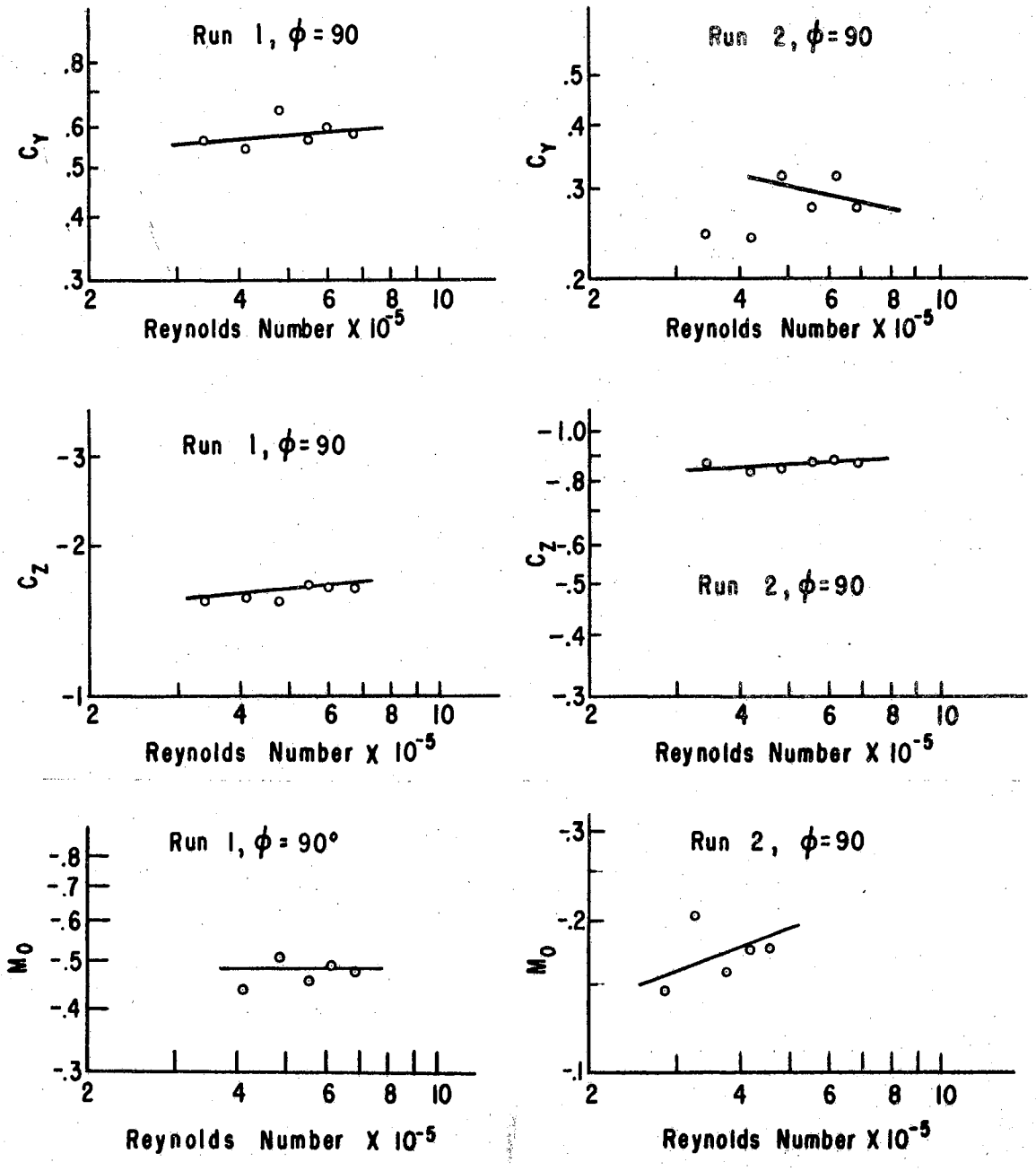

Figure 13: Effect of Reynolds' Number for Run 1 and Run 2, Ø=90

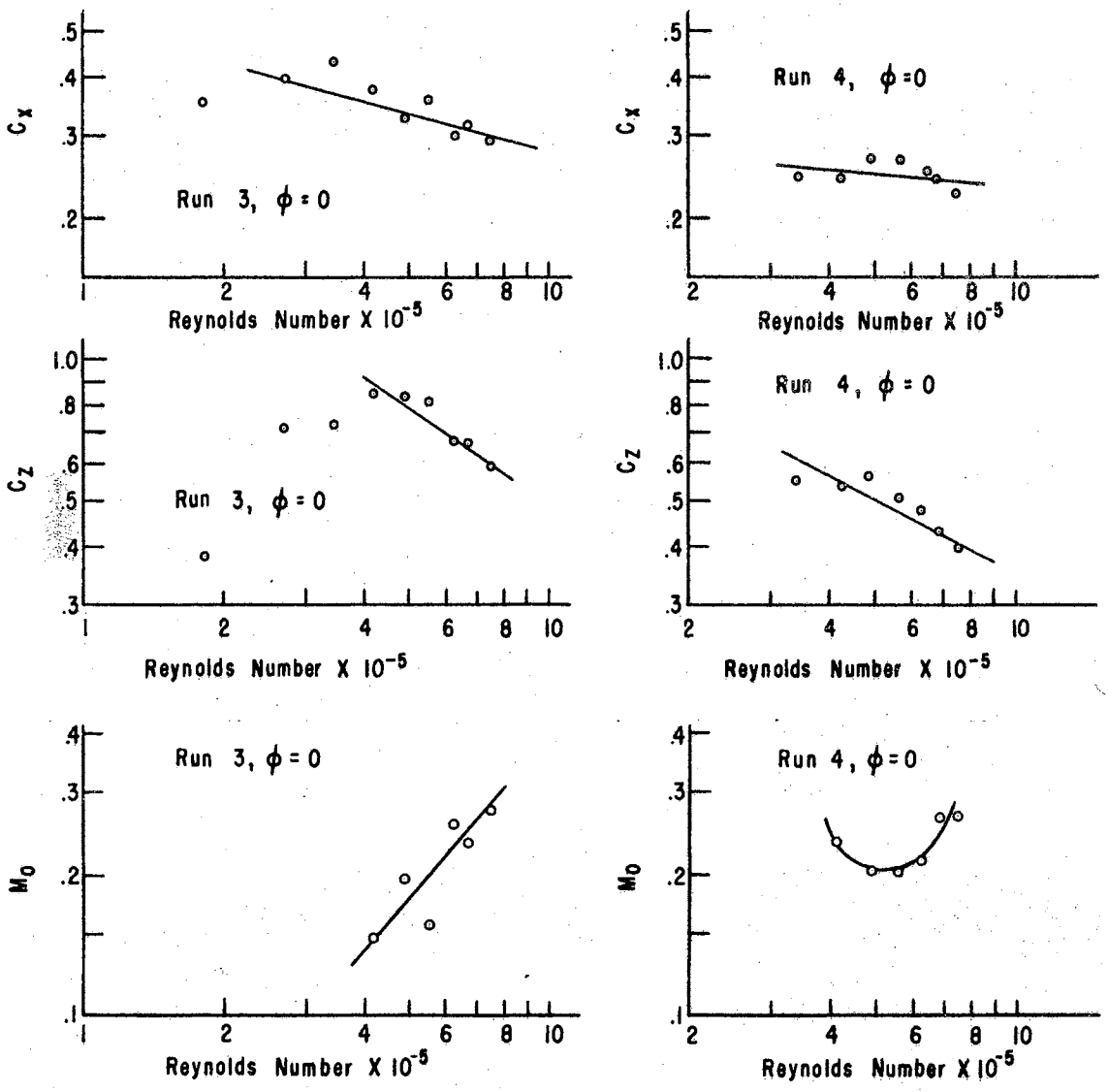

Figure 14: Effect of Reynolds' Number for Run 3 and Run 4, $\phi=0$

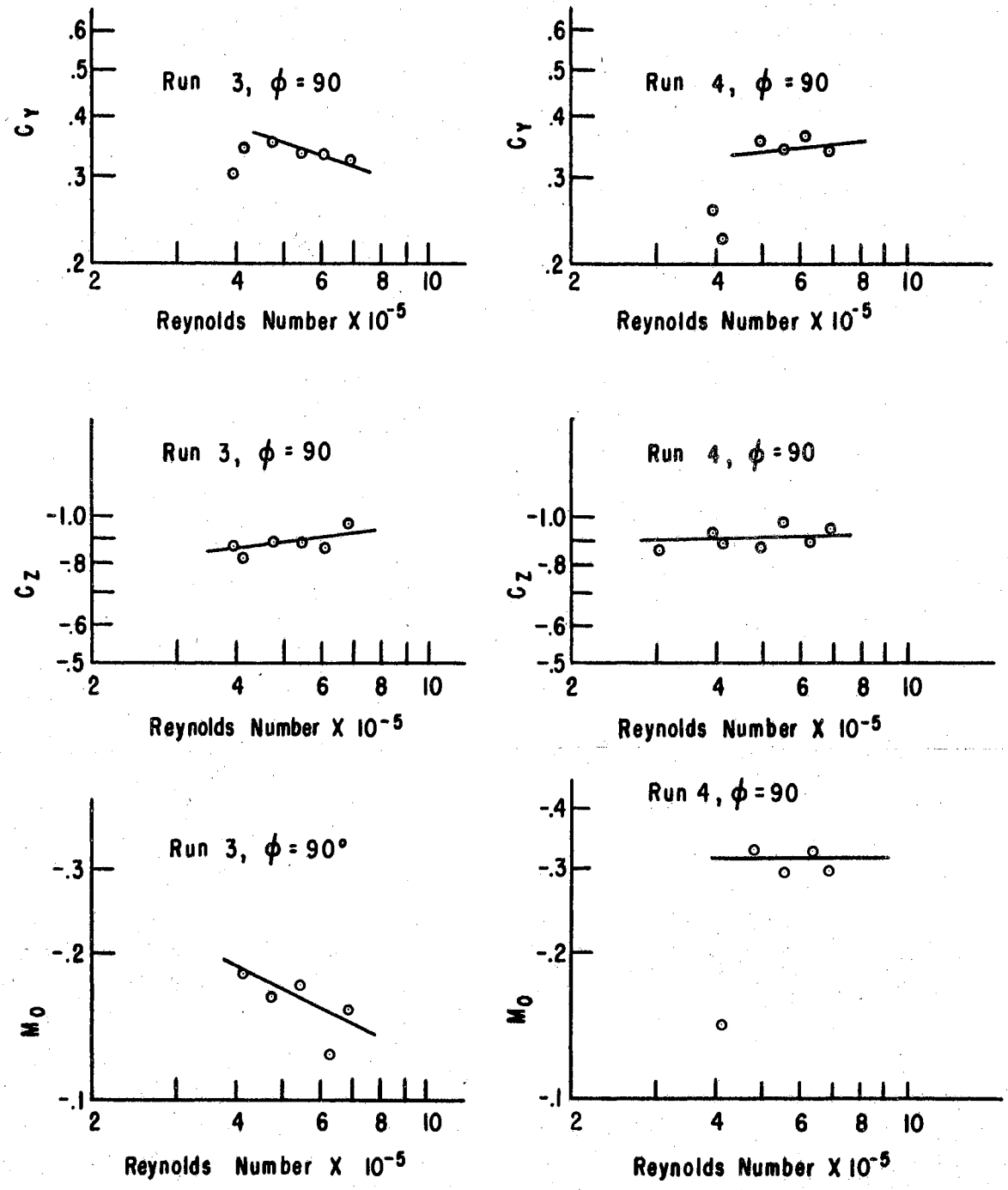

Figure 15: Effect of Reynolds' Number for Run 3 and Run 4, Ø=90

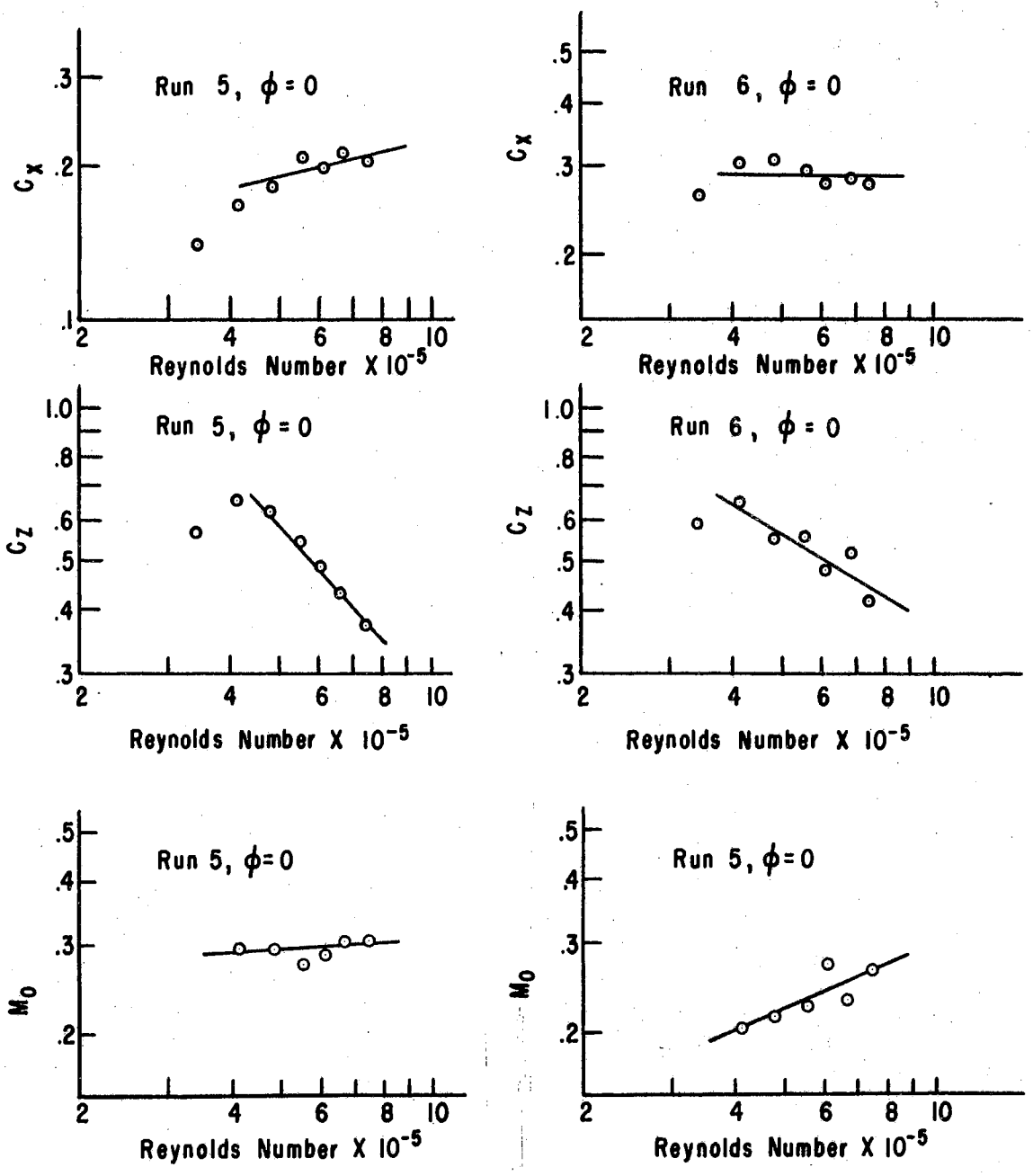

Figure 16: Effect of Reynolds' Number for Run 5 and Run 6, Ø=0

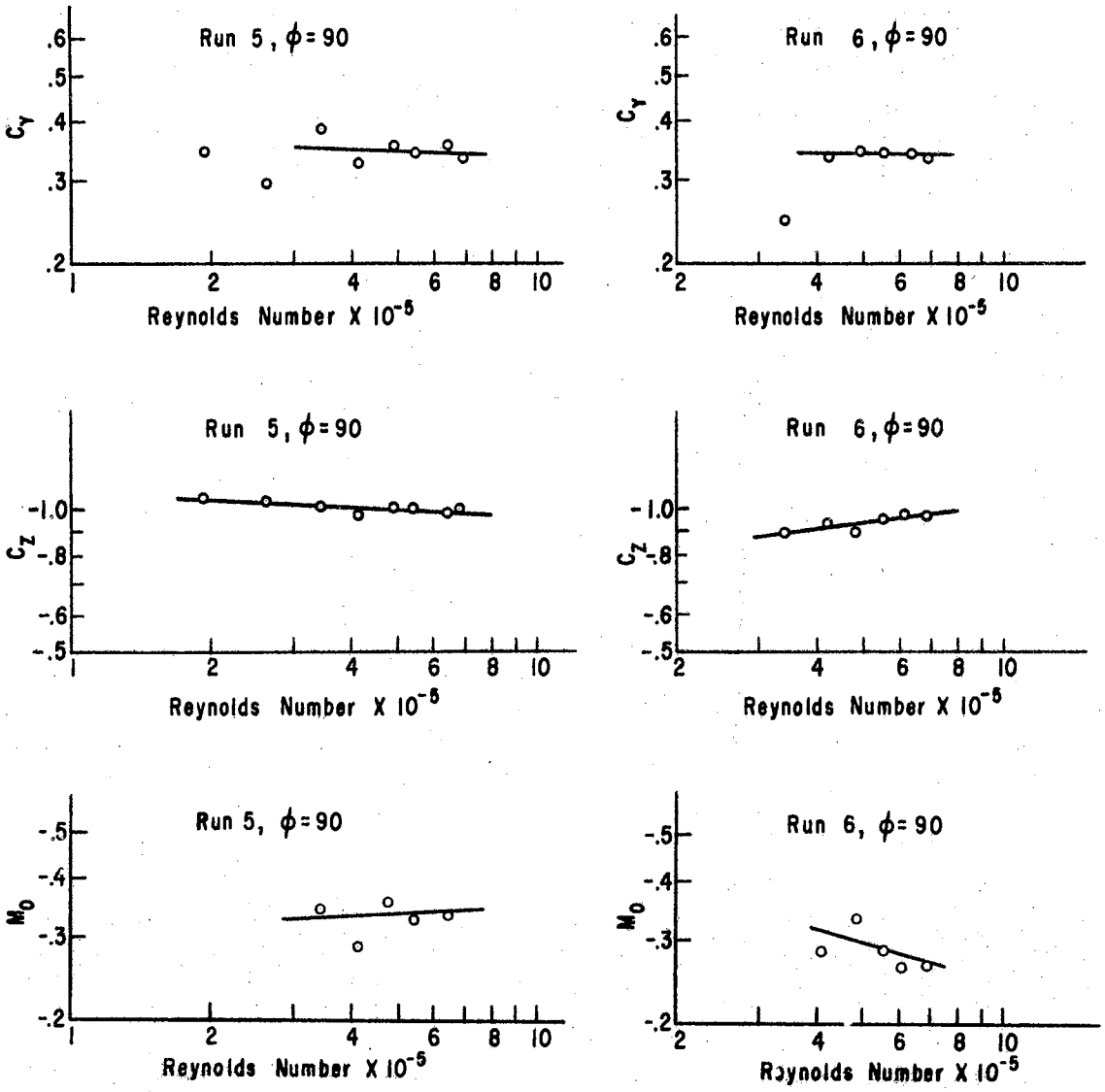

Figure 17: Effect of Reynolds' Number for Run 5 and Run 6, Ø=90

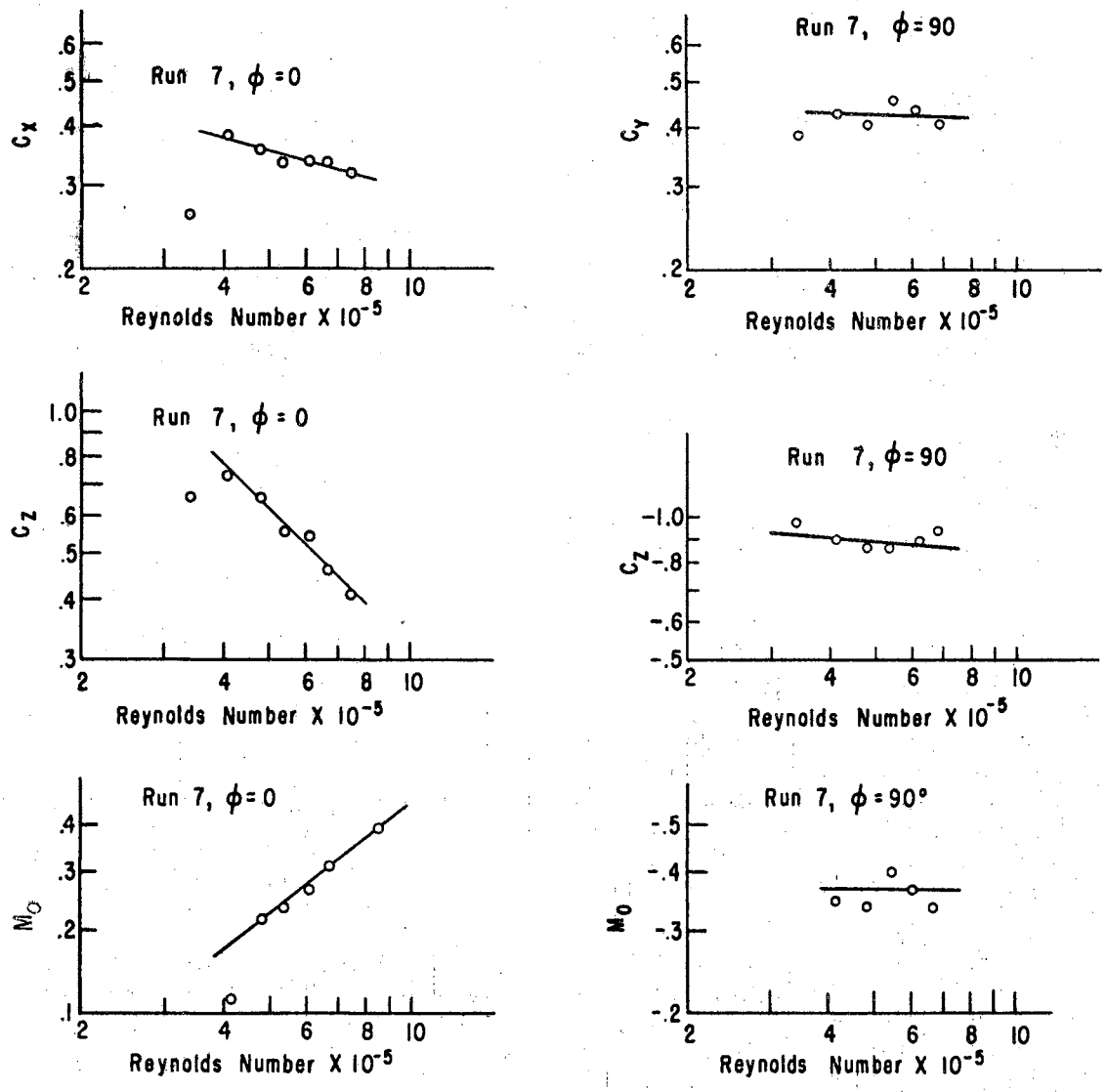

Figure 18: Effect of Reynolds' Number for Run 7, Ø=0 and Ø=90

Ø=90

The drag and lift coefficients showed very little dependency on changes in Reynolds' number above 4×10^5. The ratios of the maximum to minimum observed values were all less than 1.2. The negative value of C_z means the resultant vertical force is upward. M_o, the moment coefficient was variable with changes in Reynolds' number. No general trend was evident. The negative value of M_o means the resultant moment is trying to twist the shell down on the windward side of the shell, i.e., into the wind. The signs associated with C_z and M_o indicate that the resultant vertical force and the overturning moment are acting in opposite directions for Ø=90 than when Ø=0.

The values of the coefficients below $R_N = 4 \times 10^5$ were erratic. This was probably due to friction in the force sensing equipment.

For values of Reynolds' number investigated above the lower limit (cf. Table IV) the plots of the drag and lift coefficients appeared to be a straight line on log-log paper. The general form of such a relationship may be expressed:

$$\text{Coefficient} = a(R_N)^b$$

Tables IV and V give the values of the constant, a, and the exponent, b, determined by a linear regression analysis. The analysis was carried out for all observed points above the value of R_N given in the tables as the "lower limit." The true value of R_N is the tabulated value multiplied by 10^5. Also tabulated are the maximum and minimum values of the coefficient observed for the range in which the equation was determined.

TABLE IV
DRAG COEFFICIENT EQUATION CONSTANTS FOR Ø=0 AND Ø=90

Test Conditions			Drag Coef., C_x, Ø=0				Drag Coef., C_y, Ø=90			
Run	H/W	D/W	a	b	Range of Coef. Observed	Lower Limit of R_N	a	b	Range of Coef. Observed	Lower Limit of R_N
3	1/12	.30	10.89	-.265	.43-.29	1.9	25.67	-.327	.36-.32	4.8
2	1/10	.30	1225	-.649	.36-.18	4.2	5.148	-.216	.32-.27	4.9
5	1/8	.20	.00820	.240	.18-.21	4.8	.6019	-.042	.36-.32	3.5
4	1/8	.30	.7737	-.084	.27-.22	3.5	.7208	-.118	.34-.37	4.8
6	1/8	.40	.2463	-.005	.31-.27	3.5	.4336	-.018	.35-.33	4.8
7	1/8	.50	11.61	-.266	.38-.32	4.2	.6345	-.031	.45-.40	4.1
1	1/6	.30	15.06	-.308	.32-.25	2.7	.2047	.078	.54-.64	3.4

TABLE V
LIFT COEFFICIENT EQUATION CONSTANTS FOR Ø=0 AND Ø=90

Test Conditions			Lift Coef., C_z, Ø=0				Lift Coef., C_z, Ø=90			
Run	H/W	D/W	a	b	Range of Coef. Observed	Lower Limit of R_N	a	b	Range of Coef. Observed	Lower Limit of R_N
3	1/12	.30	5045	-.668	.84-.59	4.2	.1574	.131	.82-.96	3.4
2	1/10	.30	227.7	-.463	.61-.41	4.2	.4534	.047	.83-.88	3.4
5	1/8	.20	1183400	-1.106	.62-.37	4.8	2.044	-.055	1.06-.97	1.9
4	1/8	.30	947.7	-.572	.56-.39	4.2	.6536	.026	.87-.98	3.4
6	1/8	.40	1388	-.595	.65-.41	4.2	.2062	.115	.89-.97	3.4
7	1/8	.50	231480	-.978	.73-.41	4.2	2.703	-.084	.97-.85	3.4
1	1/6	.30	2521	-.651	.63-.41	3.5	.4984	.091	1.55-1.66	3.4

Slope Parameter Effects

Graphs of the force and moment coefficients were plotted against the slope parameter, π_7 = H/W, and are presented in Figure 19. Since Reynolds' number was effective for most of the tests, the value of each coefficient was determined for four different values of R_N.

Ø=0

The maximum value of the drag coefficient, C_x, was 0.36 corresponding to $R_N = 4 \times 10^5$ and was observed with H/W = 1/12, the flattest shell slope tested. For $R_N = 7 \times 10^5$ the maximum value of C_x was 0.30. C_x decreased as the slope ratio increased to 1/10 for all values of R_N. The minimum value was 0.19 corresponding to $R_N = 7 \times 10^5$ compared to 0.28 for $R_N = 4 \times 10^5$. For the steeper slopes of 1/8 and 1/6, C_x was approximately constant at a value of 0.25 for all values of R_N.

The lift coefficient, C_z, was also maximum for H/W = 1/12. The maximum observed values were 0.92 and 0.62 corresponding to $R_N = 4 \times 10^5$ and 0.44 for $R_N = 7 \times 10^5$, at a slope ratio of 1/10. C_z then remained about constant for the steeper slope ratios of 1/8 and 1/6. The maximum observed values were approximately 1.6 times greater than minimum observed values for a constant shell slope ratio due to Reynolds' number effects.

The moment coefficient increased with increasing shell slope. The maximum value was 0.36 corresponding to an H/W ratio of 1/6 and a Reynolds' number of 7×10^5. The minimum value of 0.14 was observed for $R_N = 4 \times 10^5$ at a slope of 1/12.

Ø=90

As the slope increased from H/W = 1/12 the drag coefficient C_y, first

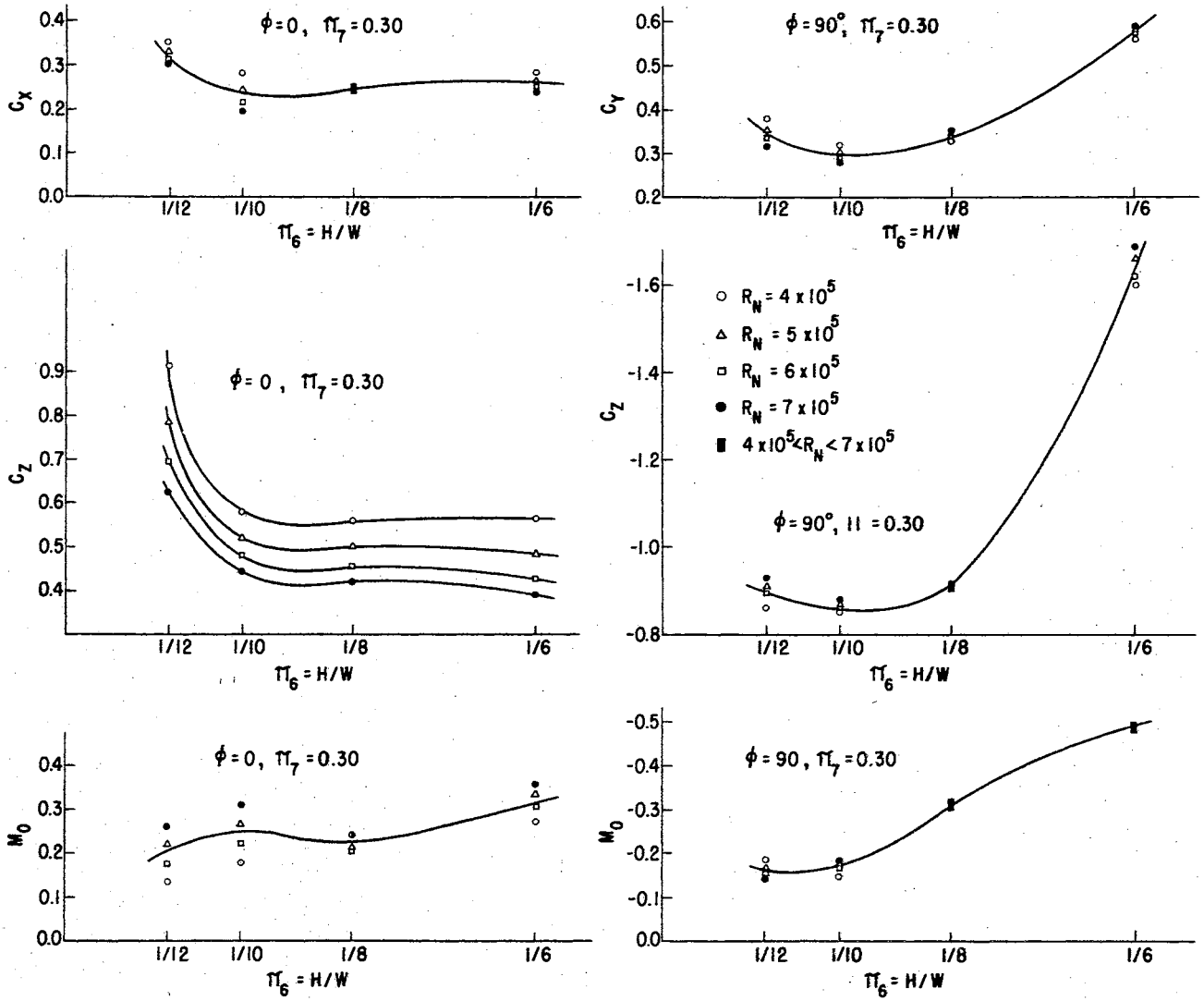

Figure 19: Slope Parameter Effects on the Force and Moment Coefficients

decreased from 0.38 to a minimum of about 0.32 for H/W = 1/10 and a value of Reynolds' number equal to 4×10^5. C_y then increased to a maximum value of around 0.58 for H/W = 1/6, the steepest slope tested.

The lift coefficient, C_z, also first declined with increasing shell slope to a minimum value at about H/W = 1/10. C_z then increased with increasing shell slope to its maximum for H/W = 1/6. The maximum and minimum values were 1.68 and 0.85.

The moment coefficient was also maximum for H/W = 1/6, the steepest shell slope. For a Reynolds' number of 7×10^5 the minimum value was 0.14 for H/W = 1/12. M_o then increased to 0.49 for a slope ratio of 1/6.

Height Parameter Effects

Graphs of the variation of the force coefficients for changes in the height parameter, π_7 = D/W, are presented in Figure 20. For most tests, variation of the height of the shell above the tunnel floor did not cause as large a change in the observed force coefficients as did the variation of the shell slope.

$\phi=0$

The increase of the drag coefficient, C_x, was approximately linear with increasing height. The range of observed values was from 0.18 to 0.38, corresponding to π_7 values of 0.20 and 0.50 respectively.

C_z, the lift coefficient was very dependent on Reynolds' number. Variation of the height of the shell caused different effects on C_z for each value of R_N. For the largest value of Reynolds' number, $R_N = 7 \times 10^5$, the lift coefficient increased with increasing height. As D/W varied from 0.2 to 0.4, C_z increased from 0.41 to 0.51. The value of C_z then decreased to 0.49 for a π_7 value of 0.50. For $R_N = 4 \times 10^5$, C_z declined from 0.75

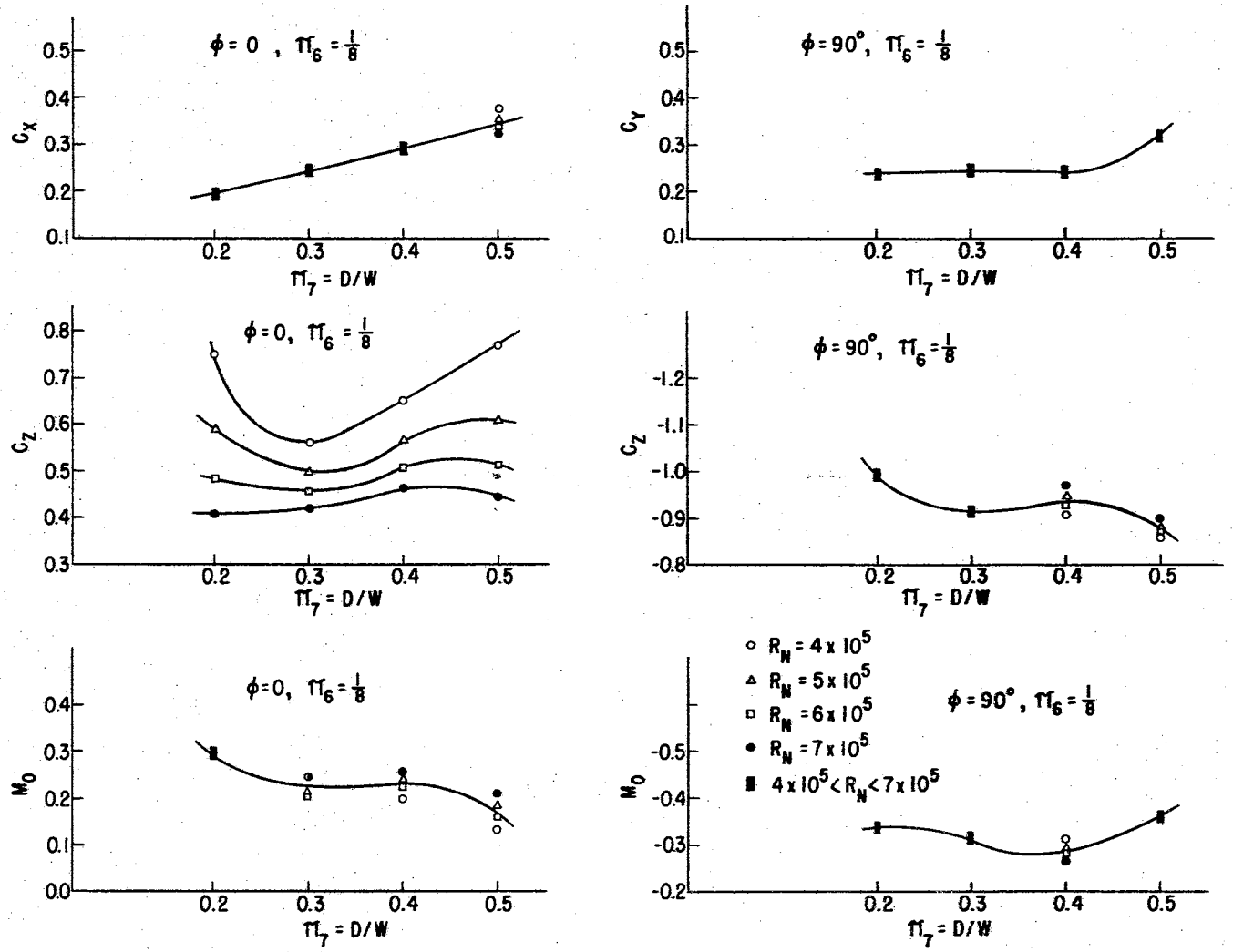

Figure 20: Height Parameter Effects on the Force and Moment Coefficients

to 0.56 as the height parameter varied from 0.20 to 0.30. C_z then increased with increasing shell height to a value of 0.76 for D/W = 0.50.

M_o, the moment coefficient was maximum for D/W = 0.20 corresponding to the minimum test height. As D/W increased, M_o decreased. The range of observed values was 0.30 to 0.13.

Ø=90

Variation of the height of the model had little effect on any of the coefficients with Ø=90. The difference between maximum and minimum observed values was usually limited to about 0.10.

The drag coefficient, C_y, was constant at approximately 0.34 from D/W = 0.20 to 0.40. C_y then rose to a maximum value of 0.42 for D/W = 0.50.

The lift coefficient, C_z, varied from 1.0 to 0.85. The maximum value occurred at the lowest height of the shell, i.e., D/W = 0.20.

M_o decreased with increasing height up to a value of D/W = 0.40 corresponding to an M_o value of about 0.28. Then the moment coefficient increased to the maximum observed value of 0.36 for D/W = 0.50.

The maximum and minimum observed values of the coefficients for all shell slope and height parameter combinations are tabulated in Table VI.

TABLE VI
MAXIMUM AND MINIMUM OBSERVED VALUES OF THE FORCE COEFFICIENTS FOR ALL TEST CONDITIONS

Test Conditions			Coefficients for Ø=0						Coefficients for Ø=90					
Run	H/W	D/W	C_x		C_z		M_o		C_y		C_z		M_o	
			Max.	Min.	Max.	Min.	Max.	Min.	Max.	Min.	Max.	Min.	Max.	Min.
3	1/12	.30	.43	.29	.84	.38	.27	.15	.36	.30	-.97	-.82	-.18	-.12
2	1/10	.30	.36	.18	.60	.42	.33	.19	.32	.24	-.88	-.84	-.20	-.14
5	1/8	.20	.21	.14	.63	.37	.31	.27	.38	.30	-1.06	-.97	-.35	-.29
4	1/8	.30	.27	.22	.56	.39	.27	.20	.37	.11	-1.08	-.83	-.33	-.19
6	1/8	.40	.31	.26	.63	.41	.27	.21	.38	.25	-.98	-.89	-.33	-.26
7	1/8	.50	.38	.26	.73	.41	.25	.11	.45	.39	-.97	-.86	-.39	-.33
1	1/6	.30	.50	.25	.61	.40	.33	.24	.62	.54	-1.73	-1.54	-.52	-.44

Barrier Effects

The following schedule of tests was set up to determine the effects of a solid barrier of height B placed at a distance S upwind from the shell model.

TABLE VII
PARAMETER COMBINATIONS TO STUDY
BARRIER EFFECTS

Run	π_6 = H/W	π_7 = D/W	π_9 = B/D	π_{10} = S/D
8	1/6	0.30	1/2	4
9	1/10			
10	1/12			
11	1/8	0.20		
12				
13		0.40		
14		0.50		
15		0.30	1/4	
16			3/4	
17			1.0	
18			1/2	6
19				8
20				10

Runs 8, 9, 14, 15, 16, and 17 were the only tests completed. Severe oscillations of the models caused such large variation in the amplitude of the oscillograph traces that the data obtained for the forces acting on the shell models was unreliable. If the sensitivity of the recorder was reduced enough to minimize the amplitude of the traces, the deflection from the null position was very small because of the small forces involved.

The drag and lift coefficients were calculated for each of the tests with barriers. The range of observed values is tabulated in Table VIII along with the range of observed values for test runs which had the same values of π_6 and π_7 but with no barrier. The ratios of the coefficients for tests with barriers to the coefficients for tests without barriers were calculated. The maximum and minimum values are tabulated in Table VIII.

TABLE VIII
COMPARISON OF FORCE COEFFICIENTS FOR TEST
WITH AND WITHOUT BARRIERS

With Barrier			Without Barrier			Ratio Barrier/ No Barrier	
Test Run	Drag, C_x	Lift, C_z	Test Run	Drag, C_x	Lift C_z	Drag	Lift
8	.070-.087	1.02-1.13	1	.25-.32	.41-.63	.22-.35	1.6-2.8
9	.030-.120	.932-1.08	2	.18-.36	.41-.61	.084-.67	1.5-2.6
14	.065-.100	1.31-1.52	7	.32-.38	.41-.73	.17-.31	1.8-3.6
15	.157-.219	.670-.770	4	.22-.27	.39-.56	.58-.99	1.2-2.0
16	.011-.089	.418-.562	4	.22-.27	.39-.56	.041-.40	.75-1.4
17	.027-.163	.111-.247	4	.22-.27	.39-.56	.10-.74	.20-.63

The drag coefficients for test runs with barriers were always less than for tests without barriers. However, the lift coefficient was as much as 3.6 times greater for tests with a barrier present equal to 1/2 the height of the shell height, i.e., $\pi_9 = 1/2$. For π_9 values of 3/4 and 1.0, both the drag and lift coefficients were reduced. Runs 15, 16, and 17 with barriers present compared to Run 4 without a barrier shows that as barrier height increases from a height equal to 1/2 the shell height, the lift coefficient decreases.

CHAPTER VII

DISCUSSION AND INTERPRETATION OF RESULTS

Prandtl and Tietjens (1934) state that for each particular body there belongs a characteristic function , $c = f(R_N)$; where c is the drag coefficient of the body. The lift and overturning moment coefficients may also be expressed as functions of Reynolds' number. These functions can be ascertained only by experiment and for each shape and position of the body the experiment must be repeated.

The flow pattern of a fluid about an object may also depend on Reynolds' number. Geometrically similar flow about geometrically similar objects is assured if the values of Reynolds' number are equal. However, it has been observed that for some objects, the variation of Reynolds' number through a certain range does not cause a change in the flow pattern. For that range of Reynolds' number the shape of the flow pattern is then independent of Reynolds' number effects.

The coefficients determined for the shell models were in most cases dependent on Reynolds' number, therefore the flow pattern about the shells was changing with increasing velocity. The function, $f(R_N)$ for the drag and lift coefficients was approximated by a linear relation on log-log paper for values of Reynolds' number between 4×10^5 and 8×10^5.

A common effect on the flow pattern with changing Reynolds' number is the variation of the location at which the boundary layer of flow separates from the object. For a thin flat plate with the flow perpendicular to the

plane of the plate, separation would occur at the edges. As the plate is rotated and the flow becomes parallel to its plane the boundary layer would cling to the surface for some length along the plate before separation would occur. This length necessary for sufficient energy dissipation to cause separation would depend on the angle of the plate with respect to the wind and the velocity of the wind, i.e., Reynolds' number. In the light of the foregoing explanation, it appears that the slopes of the shells tested were of such a value that the force coefficients were dependent on Reynolds' number.

Changing the direction of the wind flow impinging on the shell model from $\emptyset$=0 to $\emptyset$=90 caused a reversal in the direction of the resultant vertical force, R_z, and the overturning moment, M.

Variation of the slope of the shell, H/W ratio, caused significant changes in the force coefficients observed. The effect of increasing the slope was opposite for $\emptyset$=0 and $\emptyset$=90, i.e., the largest values of the lift and drag coefficients were observed with the least shell slope with $\emptyset$=0 and with the greatest shell slope with $\emptyset$=90.

The following hypothetical explanation of the action of the wind forces on the shell is presented in an attempt to qualitatively explain some of the observed wind force characteristics. Consider the two sections of the shell shown in Figure 21 to be the critical sections, i.e., the sections of the shell which most affect the magnitude and direction of the wind forces acting on the shell. For $\emptyset$=0 the flow beneath the shell probably governs the forces acting on the shell since the upper surface of the shell at the critical section is not in direct contact with the air flow. The opposite would then be the case for $\emptyset$=90 and flow above the shell would be the more important. As the air passes over the shell, the forces would be developed

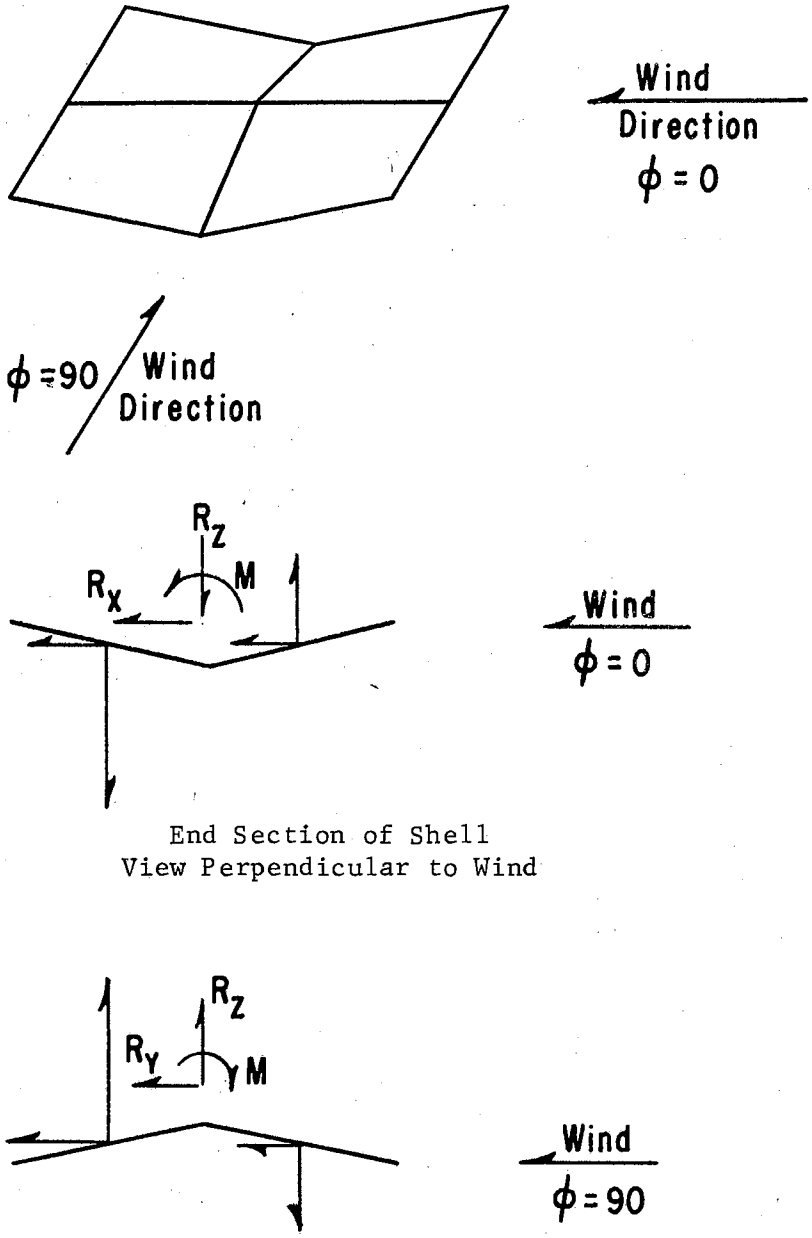

Figure 21: Sketches Showing the Theoretical and Observed Wind Forces Acting on a Hyperbolic Paraboloid Shell

on the front and rear portions of the shell in the directions shown causing the resultant force system shown at a point in the center of the shell. As the slope increases for $\emptyset$=0, the air stream beneath the shell would tend to move toward the center portion of the shell. This means less air is passing over the "critical" sections causing a reduction in the drag and lift components for shells with steep slopes. For $\emptyset$=90 the wind flow above the shell is also moved toward the center of the shell as the slope increases. This causes a larger amount of air to flow over the "critical" section of the shell increasing the drag and lift forces developed.

Changing the height of the shell model above the tunnel floor caused only small variations of the force coefficients. This was expected due to the nearly constant wind velocity profile present in the wind tunnel. The effects which were noted were probably due to interference of the wind flow beneath the model.

Although Reynolds' number in many cases was effective, the observed values of the force coefficients can be used as a guide in the design of full scale structures. Most of the coefficients were approximately constant or decreasing with increasing Reynolds' number; therefore the direct application of the observed coefficients should result in a conservative design. For tests such as Runs 1,4,5,6, and 7 with $\emptyset$=90, the drag and lift coefficients were nearly independent of Reynolds' number effects and the observed coefficients could be directly applied for the design of full scale structures.

CHAPTER VIII

SUMMARY AND CONCLUSIONS

A model study of the wind forces acting on saddle-shaped hyperbolic paraboloid shell models was conducted, (cf. Figure 1, page 3). The models were tested in a low speed wind tunnel. The experimental investigation was organized and conducted according to the principles of similitude.

Equipment was developed and a method devised for the direct determination of the force components acting on the shell models. The resultant force system was described in terms of three components; the horizontal drag, vertical lift, and overturning moment acting on the structural model.

The wind forces acting on the hyperbolic paraboloid shell models were dependent on Reynolds' number for one direction of wind flow over the shell, i.e., $\emptyset$=0, (cf. Figure 2, page 17). For some of the shell configurations with $\emptyset$=90 the drag and lift coefficients were found to be independent of Reynolds' number effects.

The directions of the vertical force and overturning moment acting on the shell were dependent on the direction of the impinging wind. The resultant vertical force was down for $\emptyset$=0 and upward for $\emptyset$=90. The direction of the overturning moment was also reversed when the direction of the wind changed from $\emptyset$=0 to $\emptyset$=90.

The slope of the shell was a more important factor in determining the force coefficients than was the height of the shell above the tunnel floor.

Solid upwind barriers caused oscillatory forces on the shell models. For all conditions tested the barriers reduced the drag coefficient. The lift coefficient was increased for barrier heights equal to 1/2 the shell height or less. For barrier heights equal to 3/4 the shell height or more the lift coefficient was reduced.

The maximum observed values of the drag, lift and overturning moment coefficients for the entire series of tests occurred for test Run 1 with $\emptyset$=90. Run 1 corresponds to a shell slope parameter of 1/6, which is the ratio of the rise to width of the shell. The shell height parameter for Run 1 was 0.30, which is the ratio of the height of the shell above the tunnel floor to the width of the shell. The maximum values of the coefficients were:

$$\text{Drag, } C_y = 0.62$$

$$\text{Lift, } C_z = 1.73$$

$$\text{Overturning Moment, } M_o = 0.52$$

Suggestions for Future Investigations

Because Reynolds' number effects were evident in the tests conducted, a more complete investigation of the forces acting on hyperbolic paraboloid structures is needed. Such a study should be conducted with facilities capable of varying the velocity over a wide range so that the effects of Reynolds' number could be determined.

A study of the resultant wind forces for diagonal wind flow over the shells is needed to completely define the resultant forces on the shell under wind loads.

The severe oscillatory forces which were developed when solid upwind

barriers were present point out the need for an investigation of the effect of such barriers on the wind stream characteristics. Such information could then be used for the design of other structural configurations.

SELECTED BIBLIOGRAPHY

Biggs, J. M. et al. "Wind Forces on Structures." Transactions, American Society of Civil Engineers. 126: Part II. Paper No. 3269. 1961.

Bridgman, P. W. Dimensional Analysis. Rev. ed. New Haven: Yale University Press, 1931.

Brooks, Fredrick A. An Introduction to Physical Microclimatology. Davis, California: University of California, 1959.

Castleman, Francis L. et al. "Discussions of Wind Load Standards in Europe." Proceedings, American Society of Civil Engineers. 77: No. D-42, 1-9. 1951.

Durst, C. S. "Duration of Wind Loadings on Buildings." Engineering (London) 188: pp. 550-2. November, 1959.

Friesen, J. F. "Wind Uplift Forces on Open Shelters." American Society of Agricultural Engineers National Student Journal. 1962.

Geiger, Rudolph. The Climate Near the Ground. Translated by Milroy Stewart and others. Cambridge, Mass.: Harvard University Press, 1950.

Haddon, J. D. "The Use of Wind Tunnel Models for Determining the Wind Pressure on Buildings." Civil Engineering and Public Works Review (London). 65: No. 645. April, 1960.

Hoerner, S. F. Fluid-Dynamic Drag. Midland Park, N. J.: by author, 1958.

Irminger, J. O. V., and Nøkkentved, Chr. Wind-Pressure on Buildings. Experimental Researches, (second series). Translated by Alexander C. Jarvis and O. Brødsgaard, Denmarks Naturvidenskabelige Samfund. Ingeniørvidenskabelige Skrifter. A, Nr. 42. Copenhagen, Denmark. 1936.

Murphy, Glen. Similitude in Engineering. New York: The Roland Press Co., 1950.

Nelson, G. L. Wind Effects on Open-Front Livestock Shelters. Ph. D. Dissertation. Iowa State College Library, 1957.

Nelson, G. L. and H. Giese. "Wind Load Reactions in Open-Front Shelters." Agricultural Engineering 43: No. 3, March, 1962.

Pagon, W. W. et al. "Discussion of Variation of Wind Velocity and Gusts with Height." Proceedings, American Society of Civil Engineers. 79: D-126, 1-20. 1953.

Prandtl, Ludwig. Essentials of Fluid Dynamics. New York: Hafner Publishing Co., 1952.

Prandtl, L. and O. G. Tietjens. Applied Hydro-and Aeromechanics. Translated by J. P. Den Hartog. 1st ed. New York and London: McGraw-Hill Book Company, Inc., 1934.

Price, P. "Suppression of Fluid-Induced Vibration of Circular Cylinders." Proceedings, American Society of Civil Engineers. 82: Paper No. 1030. EM 3, July, 1956.

Rice, C. E. Wind Forces on Open or Umbrella-Type Shelters. M. S. Thesis. Oklahoma State University Library, 1961.

Scruton, C. "Aerodynamic Buffeting of Bridges." The Engineer (London). 199: pp. 654-7. May, 1955.

Sherlock, Rotlo. "Variation of Wind Velocity and Gusts with Height." Proceedings, American Society of Civil Engineers. 78: No. 126, pp. 1-26. 1952.

Sutton, O. G. Micrometerology. New York: McGraw-Hill Book Company, Inc., 1953.

Teter, N. C., L. W. Neubauer, and J. H. Pedersen. "Farm Building Construction Standards." Paper No. 63-909. St. Joseph, Michigan: American Society of Agricultural Engineers, 1963.

Thom, H. C. S. "Distribution of Extreme Winds in the United States." Proceedings, American Society of Civil Engineers. 86: No. ST 4, April, 1960.

Van Erp, John W. T. "Wind Load Standards in Europe." Proceedings, American Society of Civil Engineers. 76: No. 42, 1-11. 1950.

APPENDIX

ORIGINAL DATA FOR TESTS CONDUCTED WITHOUT A BARRIER

RUN 1 ϕ=0

RELATIVE VELOCITY ρV^2	MEASURED FORCES - (grams) HORIZONTAL F_{XA}	F_{YB}	F_{YC}	VERTICAL F_{ZA}	F_{ZB}	F_{ZC}	RESULTANT R_X	R_Y	R_Z
70.05	186-	111-	088	142-	0606	112-	186-	023-	0352
102.31	265-	182-	201	204-	0910	157-	265-	019	0549
139.34	297-	182-	188	306-	1172	225-	297-	006	0641
176.93	424-	243-	264	407-	1536	225-	424-	021	0904
224.57	446-	202-	200	509-	1941	450-	446-	002-	0982
69.42	206-	116-	151	122-	0606	112-	206-	035	0472
104.69	276-	167-	226	224-	0930	180-	276-	059	0526
137.21	350-	192-	232	367-	1213	225-	350-	040	0621
178.35	382-	182-	226	407-	1536	360-	382-	044	0769
227.69	615-	192-	251	733-	1860	360-	615-	058	0767
71.62	223-	111-	106	142-	0667	135-	223-	005-	0390
103.50	276-	132-	138	224-	0930	180-	276-	006	0526
142.94	361-	152-	138	326-	1294	225-	361-	014-	0743
178.92	446-	192-	138	448-	1577	360-	446-	054-	0769
226.41	573-	253-	226	652-	2022	540-	573-	027-	0830

RUN 2 ϕ=0

RELATIVE VELOCITY ρV^2	MEASURED FORCES - (grams) HORIZONTAL F_{XA}	F_{YB}	F_{YC}	VERTICAL F_{ZA}	F_{ZB}	F_{ZC}	RESULTANT R_X	R_Y	R_Z
98.95	111-	055-	085	081-	0465	067-	111-	030	0317
137.37	093-	049-	045	163-	0627	090-	093-	004-	0374
180.42	212-	101-	085	163-	0768	135-	212-	016-	0470
221.09	286-	132-	076	244-	0970	157-	286-	056-	0569
270.37	403-	192-	214	402-	1213	225-	403-	022	0581
320.65	334-	101-	188	530-	1415	270-	334-	087	0615
100.02	170-	101-	126	102-	0465	090-	170-	025	0273
138.57	154-	081-	126	122-	0647	135-	154-	045	0390
178.70	191-	081-	126	204-	0788	112-	191-	045	0472
220.47	228-	099-	126	244-	0930	225-	228-	027	0461
256.29	265-	111-	189	285-	1132	225-	265-	078	0622
312.31	308-	121-	189	407-	1375	360-	308-	068	0608
98.22	223-	132-	182	102-	0455	056-	223-	050	0297
140.93	239-	121-	182	122-	0627	090-	239-	061	0415
180.97	297-	137-	182	204-	0788	090-	297-	045	0494
222.03	318-	172-	251	285-	1011	157-	318-	079	0569
272.00	340-	152-	182	326-	1213	225-	340-	030	0662
323.05	350-	182-	251	407-	1455	360-	350-	069	0688

RUN 3 $\emptyset$=0

RELATIVE VELOCITY ρV^2	MEASURED FORCES - (grams) HORIZONTAL F_{XA}	F_{YB}	F_{YC}	VERTICAL F_{ZA}	F_{ZB}	F_{ZC}	RESULTANT R_X	R_Y	R_Z
100.86	149-	132-	065	041-	0485	011-	149-	067-	0433
137.43	223-	121-	050	081-	0647	067-	223-	071-	0499
174.79	260-	126-	055	081-	0829	067-	260-	071-	0681
222.51	224-	081-	058	244-	1011	180-	224-	023-	0587
234.92	350-	162-	065	163-	1051	090-	350-	097-	0798
305.60	403-	202-	163	204-	1375	225-	403-	136-	0946
100.28	233-	121-	058	041-	0465	067-	233-	087-	0425
137.75	244-	111-	055	061-	0606	090-	244-	056-	0455
177.85	318-	152-	075	061-	0809	090-	318-	077-	0658
220.02	424-	238-	201	122-	1011	135-	424-	037-	0754
259.46	403-	182-	201	204-	1213	225-	403-	019	0784
328.15	467-	213-	151	285-	1455	315-	467-	062-	0855
101.76	149-	075-	050	061-	0465	067-	149-	025-	0337
136.86	164-	061-	045	081-	0627	090-	164-	016-	0456
168.67	286-	101-	085	081-	0788	067-	286-	016-	0640
224.32	286-	111-	125	143-	1011	135-	286-	014	0733
273.73	382-	152-	138	244-	1213	180-	382-	014-	0789
327.08	446-	192-	188	407-	1455	180-	446-	004-	0868

RUN 4 $\emptyset$=0

RELATIVE VELOCITY ρV^2	MEASURED FORCES - (grams) HORIZONTAL F_{XA}	F_{YB}	F_{YC}	VERTICAL F_{ZA}	F_{ZB}	F_{ZC}	RESULTANT R_X	R_Y	R_Z
99.47	164-	234-	132	092-	0566	090-	164-	102-	0384
128.55	223-	244-	121	143-	0748	135-	223-	123-	0470
178.20	382-	458-	170	163-	1011	202-	382-	288-	0646
223.77	393-	458-	176	326-	1253	225-	393-	282-	0702
268.66	414-	448-	163	407-	1536	292-	414-	285-	0837
327.33	448-	489-	188	407-	1779	450-	448-	301-	0922
100.54	180-	085-	170	122-	0606	067-	180-	085	0417
138.70	233-	121-	176	122-	0809	157-	233-	054	0530
181.76	297-	152-	201	143-	1051	180-	297-	049	0728
223.59	414-	182-	226	244-	1294	270-	414-	044	0780
268.59	477-	243-	276	367-	1536	360-	477-	033	0809
326.40	488-	243-	239	489-	1860	450-	488-	004-	0921
104.00	175-	061-	048	143-	0606	112-	175-	013-	0351
139.65	307-	121-	126	081-	0829	135-	307-	005	0613
182.71	328-	152-	126	244-	1011	180-	328-	026-	0587
224.82	381-	172-	176	285-	1253	225-	381-	004	0743
275.01	499-	248-	195	407-	1577	360-	499-	053-	0810
328.60	520-	243-	201	407-	1738	450-	520-	042-	0881

RUN 5 Ø=0

RELATIVE VELOCITY ρV^2	MEASURED FORCES - (grams) HORIZONTAL F_{XA}	F_{YB}	F_{YC}	VERTICAL F_{ZA}	F_{ZB}	F_{ZC}	RESULTANT R_X	R_Y	R_Z
102.84	111-	012-	020	081-	0586	090-	111-	008	0415
132.75	175-	055-	063	081-	0768	135-	175-	008	0552
180.21	255-	086-	113	204-	0970	225-	255-	027	0541
220.47	255-	081-	063	285-	1213	270-	255-	018-	0658
271.84	403-	172-	176	326-	1496	360-	403-	004	0810
331.60	552-	172-	188	407-	1819	450-	552-	016	0962
100.56	149-	042-	078	081-	0586	090-	149-	036	0415
135.24	202-	077-	093	102-	0809	140-	202-	016	0567
177.68	265-	096-	100	163-	0970	180-	265-	004	0627
220.14	308-	116-	126	204-	1212	270-	308-	010	0738
266.71	382-	162-	188	326-	1496	415-	382-	026	0755
310.91	456-	192-	226	407-	1657	450-	456-	034	0800
96.56	091-	042-	050	061-	0566	067-	091-	008	0438
137.13	143-	055-	050	122-	0788	135-	143-	005-	0531
177.35	260-	132-	138	170-	1051	180-	260-	006	0701
217.38	361-	197-	157	204-	1253	225-	361-	040-	0824
248.63	382-	182-	163	326-	1415	270-	382-	019-	0819
325.17	382-	172-	176	509-	1738	450-	382-	004	0779

RUN 6 Ø=0

RELATIVE VELOCITY ρV^2	MEASURED FORCES - (grams) HORIZONTAL F_{XA}	F_{YB}	F_{YC}	VERTICAL F_{ZA}	F_{ZB}	F_{ZC}	RESULTANT R_X	R_Y	R_Z
97.21	223-	095-	138	143-	0667	090-	223-	043	0434
133.97	340-	167-	188	244-	0890	180-	340-	021	0466
177.81	382-	162-	188	285-	1172	225-	382-	026	0662
211.08	403-	132-	138	285-	1375	315-	403-	006	0775
270.46	594-	304-	327	326-	1738	225-	594-	023	1187
317.94	679-	263-	201	509-	2022	450-	679-	062-	1063
101.92	180-	079-	138	122-	0667	090-	180-	059	0455
131.49	249-	116-	144	163-	0849	135-	249-	028	0551
180.71	350-	172-	182	204-	1132	225-	350-	010	0703
223.90	414-	192-	182	367-	1415	270-	414-	010-	0778
267.90	509-	243-	188	407-	1698	337-	509-	055-	0954
333.40	657-	304-	226	509-	2022	562-	657-	078-	0951
100.07	228-	111-	055	143-	0667	090-	228-	056-	0434
137.75	286-	137-	090	204-	0889	135-	286-	047-	0550
178.92	382-	197-	130	244-	1213	225-	382-	067-	0744
215.56	446-	202-	151	407-	1415	360-	446-	051-	0648
269.89	509-	273-	176	407-	1698	450-	509-	097-	0841
327.31	552-	283-	176	611-	2022	562-	552-	107-	0849

RUN 7 Ø=0

RELATIVE VELOCITY ρV^2	MEASURED FORCES - (grams) HORIZONTAL F_{XA}	F_{YB}	F_{YC}	VERTICAL F_{ZA}	F_{ZB}	F_{ZC}	RESULTANT R_X	R_Y	R_Z
100.94	265-	157-	121	122-	0748	112-	265-	036-	0514
135.86	340-	172-	157	204-	0991	157-	340-	015-	0630
179.97	435-	228-	182	285-	1253	270-	435-	046-	0698
221.48	594-	324-	283	367-	1577	359-	594-	041-	0851
267.67	615-	334-	276	509-	1637	450-	615-	058-	0678
329.30	743-	354-	301	611-	2224	562-	743-	053-	1051
97.62	276-	147-	214	122-	0667	067-	276-	067	0478
134.89	350-	172-	214	204-	0970	180-	350-	042	0586
173.44	467-	253-	264	204-	1213	180-	467-	011	0829
221.64	594-	263-	257	306-	1577	315-	594-	006-	0956
254.10	637-	273-	251	448-	1819	337-	637-	022-	1034
327.69	764-	344-	327	713-	2224	675-	764-	017-	0836
97.86	255-	121-	126	081-	0728	112-	255-	005	0535
134.19	329-	152-	176	143-	0930	157-	329-	024	0630
154.96	403-	137-	132	285-	1213	225-	403-	005-	0703
218.42	509-	213-	226	367-	1577	337-	509-	013	0873
268.14	615-	273-	251	407-	1819	562-	615-	022-	0850
322.59	700-	314-	276	611-	2123	562-	700-	038-	0950

RUN 1 Ø=90

RELATIVE VELOCITY	MEASURED FORCES - (grams)								
	HORIZONTAL			VERTICAL			RESULTANT		
ρV^2	F_{XA}	F_{YB}	F_{YC}	F_{ZA}	F_{ZB}	F_{ZC}	R_X	R_Y	R_Z
98.79	034-	111	163	224-	0389-	112-	034-	274	0725-
135.67	017-	162	264	306-	0544-	157-	017-	426	1007-
178.96	013-	202	276	407-	0778-	202-	013-	478	1387-
206.97	000	243	301	489-	0993-	247-	000	544	1729-
273.13	021-	323	402	652-	1167-	337-	021-	725	2156-
100.34	021-	121	060	244-	0428-	112-	021-	181	0784-
136.24	000	192	201	306-	0583-	135-	000	393	1024-
180.33	000	232	251	407-	0778-	202-	000	483	1387-
217.44	010	303	377	448-	0856-	270-	010	680	1574-
266.35	020	364	402	652-	1167-	360-	020	766	2179-
95.74	000	111	182	204-	0389-	108-	000	293	0701-
133.43	000	162	201	306-	0467-	135-	000	363	0908-
179.00	030	243	214	407-	0778-	225-	030	457	1410-
212.57	040	283	251	489-	0972-	247-	040	534	1708-
270.70	020	364	352	713-	1167-	360-	020	716	2240-

RUN 2 Ø=90

RELATIVE VELOCITY	MEASURED FORCES - (grams)								
	HORIZONTAL			VERTICAL			RESULTANT		
ρV^2	F_{XA}	F_{YB}	F_{YC}	F_{ZA}	F_{ZB}	F_{ZC}	R_X	R_Y	R_Z
101.88	006	077	048	143-	0292-	072-	006	125	0507-
137.31	020	111	138	183-	0389-	112-	020	249	0684-
179.32	000	141	176	285-	0506-	135-	000	317	0926-
219.74	010	172	188	367-	0622-	157-	010	360	1146-
272.13	010	202	251	407-	0778	225-	010	453	1267-
102.20	030-	077	065	163-	0253-	072-	030-	142	0448-
137.38	000	121	176	163-	0350-	090-	000	297	0603-
180.49	021-	141	126	285-	0467-	112-	021-	267	0864-
219.38	000	182	188	367-	0544-	157-	000	370	1068-
273.16	042-	202	151	407-	0778-	202-	042-	353	1387-
100.02	015-	097	050	143-	0272-	063-	015-	147	0478-
135.74	021-	111	075	204-	0369-	090-	021-	186	0663-
180.86	021-	152	100	285-	0467-	112-	021-	252	0864-
224.89	021-	183	126	367-	0544-	157-	021-	309	1068-
272.72	011-	232	226	407-	0778-	180-	011-	458	1365-

RUN 3 Ø=90

RELATIVE VELOCITY ρV^2	MEASURED FORCES - (grams) HORIZONTAL F_{XA}	F_{YB}	F_{YC}	VERTICAL F_{ZA}	F_{ZB}	F_{ZC}	RESULTANT R_X	R_Y	R_Z
98.26	020	073	163	163-	0233-	000	020	236	0396-
130.67	009	091	163	204-	0350-	000	009	254	0554-
178.14	040	141	176	285-	0467-	000	040	317	0752-
222.49	020	182	226	367-	0544-	000	020	408	0911-
270.70	040	202	251	489-	0856-	000	040	453	1345-
99.56	034-	049	050	183-	0214-	000	034-	099	0397-
133.92	016	111	100	244-	0331-	000	016	211	0575-
176.05	008	121	113	285-	0467-	000	008	234	0752-
219.32	011-	141	126	367-	0544-	000	011-	267	0911-
270.49	000	182	163	407-	0778-	000	000	345	1185-
101.11	004	057	095	143-	0214-	000	004	152	0357-
136.84	004	081	138	224-	0311-	000	004	219	0535-
171.97	006	101	176	285-	0389-	000	006	277	0674-
215.16	004	152	214	407-	0428-	000	004	366	0835-
273.31	010	182	251	489-	0700-	000	010	433	1189-

RUN 4 Ø=90

RELATIVE VELOCITY ρV^2	MEASURED FORCES - (grams) HORIZONTAL F_{XA}	F_{YB}	F_{YC}	VERTICAL F_{ZA}	F_{ZB}	F_{ZC}	RESULTANT R_X	R_Y	R_Z
99.96	013-	106	100	153-	0331-	112-	013-	206	0596-
136.74	042-	258	239	204-	0486-	157-	042-	497	0847-
183.18	074-	263	201	306-	0622-	225-	074-	464	1153-
232.01	053-	303	402	367-	0778-	270-	053-	705	1415-
273.03	051	344	427	448-	0875-	360-	051	771	1683-
99.25	072-	040	070	183-	0369-	124-	072-	110	0676-
132.39	064-	081	151	204-	0428-	157-	064-	232	0789-
175.64	025-	152	188	244-	0661-	225-	025-	340	1130-
221.32	021-	212	251	326-	0778-	270-	021-	463	1374-
269.89	000	303	276	489-	1089-	360-	000	579	1938-
101.12	015-	077	085	162-	0331-	117-	015-	162	0610-
136.85	021-	111	182	202-	0467-	180-	021-	293	0849-
179.14	051	202	188	243-	0583-	225-	051	390	1051-
208.40	000	242	251	324-	0778-	270-	000	493	1372-
274.70	051	283	377	445-	0972-	405-	051	610	1822-

RUN 5 Ø=90

RELATIVE VELOCITY	MEASURED FORCES - (grams)								
	HORIZONTAL			VERTICAL			RESULTANT		
ρV^2	F_{XA}	F_{YB}	F_{YC}	F_{ZA}	F_{ZB}	F_{ZC}	R_X	R_Y	R_Z
70.29	040	085	176	101-	0272-	112-	040	261	0485-
98.90	016	111	188	162-	0350-	157-	016	299	0669-
135.24	020	141	221	202-	0506-	225-	020	362	0933-
173.49	011-	202	226	324-	0700-	315-	011-	428	1339-
222.69	000	243	377	364-	0779-	405-	000	620	1548-
67.45	008	093	060	112-	0253-	112-	008	153	0477-
96.10	040-	093	163	143-	0350-	157-	040-	256	0650-
133.69	021-	141	188	204-	0544-	225-	021-	329	0973-
173.21	012	192	227	244-	0622-	270-	012	419	1136-
218.95	000	232	301	326-	0778-	360-	000	533	1464-
67.69	006	057	095	101-	0292-	112-	006	152	0505-
100.35	004-	089	038	163-	0350-	180-	004-	127	0693-
131.22	004	111	176	224-	0506-	225-	004	287	0955-
170.86	008	152	251	285-	0622-	292-	008	403	1199-
222.06	020	202	327	367-	0856-	360-	020	529	1583-
270.34	020	283	352	448-	1011-	450-	020	635	1909-

RUN 6 Ø=90

RELATIVE VELOCITY	MEASURED FORCES - (grams)								
	HORIZONTAL			VERTICAL			RESULTANT		
ρV^2	F_{XA}	F_{YB}	F_{YC}	F_{ZA}	F_{ZB}	F_{ZC}	R_X	R_Y	R_Z
101.62	000	091	138	204-	0389-	079-	000	229	0672-
134.34	028	152	214	285-	0506-	112-	028	366	0903-
177.98	024	192	226	367-	0700-	135-	024	418	1202-
220.38	040	243	251	489-	0856-	157-	040	494	1502-
269.20	051	323	352	652-	1011-	225-	051	675	1888-
98.85	016	111	126	204-	0350-	090-	016	237	0644-
133.55	012	152	232	285-	0467-	090-	012	384	0842-
173.39	000	182	276	407-	0700-	112-	000	458	1219-
211.08	000	243	276	489-	0778-	135-	000	519	1402-
271.47	000	283	364	570-	1011-	180-	000	547	1761-
99.80	017-	073	176	204-	0389-	067-	017-	249	0660-
133.97	000	152	188	265-	0428-	090-	000	340	0783-
176.37	000	192	276	367-	0622-	135-	000	418	1124-
218.24	000	222	327	611-	0778-	180-	000	549	1569-
269.87	010	283	402	652-	1011-	225-	010	685	1888-

RUN 7 Ø=90

RELATIVE VELOCITY ρV^2	MEASURED FORCES - (grams) HORIZONTAL F_{XA}	F_{YB}	F_{YC}	VERTICAL F_{ZA}	F_{ZB}	F_{ZC}	RESULTANT R_X	R_Y	R_Z
101.04	017-	101	201	285-	0350-	009-	017-	302	0644-
134.56	000	152	239	326-	0467-	022-	000	391	0815-
176.73	004	182	427	448-	0700-	034-	004	609	1182-
214.92	000	243	490	489-	0817-	045-	000	733	1351-
271.04	000	303	528	693-	0933-	067-	000	831	1693-
99.26	008	101	201	265-	0369-	013-	008	302	0647-
132.94	004-	162	214	326-	0467-	009-	004-	376	0802-
175.49	004	202	352	448-	0583-	022-	004	554	1053-
219.78	020	243	389	570-	0700-	045-	020	632	1315-
272.50	010	303	452	733-	0972-	045-	010	755	1750-
101.53	017-	152	151	244-	0350-	018-	017-	303	0612-
135.05	013-	202	176	326-	0467-	022-	013-	378	0815-
166.71	004-	222	276	407-	0467-	036-	004-	498	0910-
213.98	000	263	339	570-	0778-	045-	000	602	1393-
269.69	010	303	427	652-	1069-	067-	010	730	1788-

VITA

Karlson E. Mannschreck

Canidate for the Degree of

Master of Science

Thesis: A MODEL STUDY OF WIND FORCES ON HYPERBOLIC PARABOLOID SHELLS

Major Field: Agricultural Engineering

Biographical:

Personal Data: Born at Oklahoma City, Oklahoma, September 21, 1940, the son of Karl E. and Marie C. Mannschreck.

Education: Attended grade and high school at Union City, Oklahoma. Graduated from Union City High School in 1958; received the Bachelor of Science degree in Agricultural Engineering in January, 1963, from Oklahoma State University; completed the requirements for the Master of Science degree in May, 1964.

Professional experience: Graduate research assistant for the Agricultural Engineering Department, Oklahoma State University, for one year.